Density Functional and Ab Initio Study of Cr(CO)$_n$ ($n = 1−6$) Complexes

Joonghan Kim, Tae Kyu Kim, Jangbae Kim, Yoon Sup Lee, and Hyotcherl Ihee*

Department of Chemistry and School of Molecular Science (BK21), Korea Advanced Institute of Science and Technology (KAIST), Daejeon, 305-701, Republic of Korea

Cr(CO)$_n$ ($n = 1−6$) systems were studied for all possible spin states using density functional and high-level ab initio methods to provide a more complete theoretical understanding of the structure of species that may form during ligand dissociation of Cr(CO)$_6$. We carried out geometry optimizations for each system and obtained vibrational frequencies, sequential bond dissociation energies (BDE), and total CO binding energies. We also compared the performance of various DFT functionals. Generally, the ground states of Cr(CO)$_6$, Cr(CO)$_5$, and Cr(CO)$_4$, whose spin multiplicity is a singlet, are in good agreement with both previous theoretical results and currently available experimental data. Calculations on Cr(CO)$_3$, Cr(CO)$_2$, and CrCO provide new findings that the ground state of Cr(CO)$_3$ might be a quintet with C_{2v} symmetry instead of a singlet with C_{3v} symmetry, and the ground state of Cr(CO)$_2$ is not a linear quintet, as suggested by previous DFT calculations, but rather a linear septet. We also found that nonet states of Cr(CO)$_2$ and CrCO display partial C−O bond breakage.

Introduction

Transition metal carbonyl compounds, M(CO)$_n$, serve as building blocks in organometallic chemistry and play important roles in heterogeneous catalysis.[1,2] To understand the mechanism of such catalytic activity and to aid in the design of better catalysts, the nature of relevant reaction intermediates need to be understood. Toward this goal, there have been numerous experimental[3−6] and theoretical investigations.[7−9] Among these studies, ultrafast diffraction is unique because it can give direct structural information about reaction intermediates and reaction pathways.[3,5,6,10−16] Several organic molecules have been studied using ultrafast electron diffraction,[3,12,13,16] but organometallic molecules have received less attention.[10,11]

Due to the rich chemistry of Cr(CO)$_n$, this system is an interesting subject for ultrafast diffraction. The data obtained from such tools can be used for comparisons with theoretical values predicted by various ab initio and density functional theory (DFT) calculations, thus providing a useful database with which to judge the accuracy of each theoretical method. Depending on the excitation wavelength, all sorts of fragmented Cr(CO)$_n$ can be populated during the photodissociation of Cr-(CO)$_6$. Therefore, it is a prerequisite to have a database of all possible candidate intermediate structures that can occur during ligand dissociation of Cr(CO)$_6$.

Cr(CO)$_6$ exemplifies metal−carbonyl bonding and has been studied extensively both theoretically[17−39] and experimentally.[40−54] DFT studies at various levels have been conducted on Cr(CO)$_6$ and CrCO, and the agreement with experimental results has been demonstrated.[19,20,22,27,29,30,32−36,38,39,55−62] In addition, less attention has been paid to other unsaturated Cr(CO)$_n$ ($n = 2−5$) complexes, likely to be major photolysis intermediates of Cr-(CO)$_6$, and only a few detailed theoretical results have been reported. Li et al. calculated singlet states of Cr(CO)$_3$ and Cr-(CO)$_4$ at DFT level with double-ζ basis set, but their optimized

geometrical parameters are not shown.[63,64] Hyla-Kryspin et al. also investigated Cr(CO)$_3$ and Cr(CO)$_4$ using DFT methods and provided geometrical parameters. However, only $^1A_1$ state (C_{2v} for Cr(CO)$_4$ and C_{3v} for Cr(CO)$_3$) has been investigated although both Cr(CO)$_4$ and Cr(CO)$_3$ can adopt other symmetries.[65] Sequential bond dissociation energies (BDE) of Cr(CO)$_n$ complexes have been investigated using DFT and ab initio methods.[65] However, the previous study calculated BDEs up to Cr(CO)$_3$ and between only singlet species.[65] Obviously, there is a demand for systematic approaches to theoretical treatment. For this reason, we carried out systematic calculations on the Cr(CO)$_n$ system using both DFT and high-level ab initio calculations.

We chose DFT as our major tool, which is now widely used to determine structures and reaction energy diagrams for a variety of molecules. Compared to high-level ab initio molecular orbital theories, DFT requires less computational time and storage memory.[66,67] Moreover, the hybrid functionals give results quite close to those for high-level ab initio calculations.[55,68,69] For this reason, in this work, molecular structures, as well as vibrational frequencies and sequential bond dissociation energies of Cr(CO)$_n$ ($n = 1−6$) have been investigated through various DFT methods. The calculated results for vibrational frequency and bond dissociation energy should be useful for experimental studies.

High-level ab initio methods such as coupled cluster singles and doubles (CCSD) and CCSD with perturbed triples (CCSD-(T)) were also used for some cases where their use was critical for clarifying important issues. The calculated results were compared with the available experimental values and excellent agreement between theory and experiment in geometries and bond dissociation energies of Cr(CO)$_n$ ($n = 4−6$) was found. The high spin states of Cr(CO)$_n$ ($n = 1−4$) are also discussed. For Cr(CO)$_3$, the singlet C_{3v} structure was observed experimentally.[46,70,71] However, the lowest-energy state may have a C_{2v} symmetry with a higher spin state. In both Cr(CO)$_2$ and CrCO cases, it is of importance whether their structures are bent

* To whom correspondence should be addressed. E-mail: hyotcherl. ihee@kaist.ac.kr.
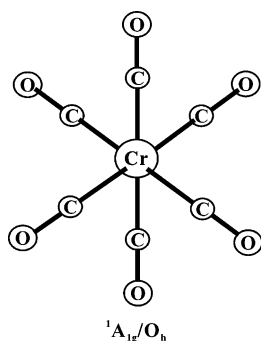
Figure 1. Molecular structure of Cr(CO)$_6$ (molecular state/molecular symmetry).

Figure 2. Molecular structures of Cr(CO)$_5$ (molecular state/molecular symmetry).

or linear. In the case of Cr(CO)$_2$, no higher-level calculation has been performed to date. For the ground state of CrCO, ab initio[58,59] and DFT[55,60,61] methods have provided results contrary to each other. The former gave a linear structure with a septet whereas the latter gave a bent structure as a septet. Recently, we demonstrated that the ground state of CrCO is a septet bent structure using the CCSD(T) method.[72] In addition, we accurately reproduced the BDE of CrCO. In this work, we extend the calculation to other spin states of CrCO. We hope this work aids further experimental studies in determining geometry and dissociation energies of Cr(CO)$_n$ ($n = 2$–5), which have not yet been available.

Computational Details

All calculations have been carried out using the Gaussian 03W and Gaussian 03 program packages.[73] We performed DFT calculations using hybrid functionals (B3LYP,[74,75] B3PW91,[74] B3P86,[74,76] mPW1PW91[77,78]) and generalized gradient approximation (GGA) functionals (BLYP,[75,79] BPW91,[78,79] BP86,[76,79] PBE[80]). The 6-311+G(3df) basis sets have been used
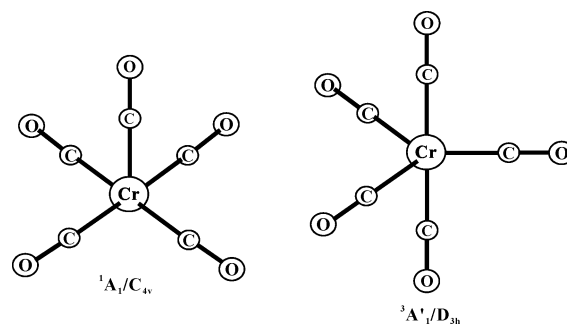
for both carbon and oxygen atom ((12s6p3d1f)/[5s4p3d1f]), whereas Wachters−Hay[81,82] all electron basis set using the scaling factors of Raghavachari and Trucks,[83] three sets of polarization functions, and a set of diffuse functions ((15s11p6d3f1g)/[10s7p4d3f1g]) have been employed for chromium. A combination of these basis sets are referred to as 6-311+G(3df). For the B3LYP functional, we performed additional calculations using the 6-311+G(d) basis set (Cr, (15s11p6d1f)/[10s7p4d1f]; C and O, (12s6p1d)/[5s4p1d]) to check for basis set dependency. The structures of possible spin states were fully optimized and subsequent harmonic vibrational frequencies have been calculated at the optimized structures. We used the restricted DFT method for singlet cases. The calculated BDE includes the corrections for zero point energies (ZPE), thermal enthalpy (298 K), and the basis set superposition error (BSSE) corrected by the counterpoise method.[84]

The calculated relative energies, BDE, full-optimized geometrical parameters and C−O stretching vibrational frequencies in Cr(CO)$_n$ are shown in Figures 1−6 and Tables 1−15. In addition, we performed the calculation of diatomic CO using various DFT functionals and ab initio methods to select an

TABLE 1: Geometrical Parameters (Lengths in Å, Angles in Deg) and Scaled C−O Stretching Vibrational Frequencies (cm^{-1}) of the $^1A_{1g}$ State of Cr(CO)$_6$ from DFT Calculations Using the 6-311+G(3df) Basis Set (in Parentheses, Calculated Results Using the 6-311+G(d) Basis Set)

$^1A_{1g}$		hybrid				GGA				exp
		B3LYP	B3PW91	B3P86	mPW1PW91	BLYP	BPW91	BP86	PBE	
geom[a]	r(Cr−C)	1.926 (1.928)	1.903	1.899	1.900	1.935	1.907	1.908	1.904	1.918[b]
	r(C−O)	1.138 (1.141)	1.138	1.137	1.136	1.153	1.151	1.152	1.152	1.141[b]
freq	A_{1g}	2096.2 (2091.8)	2102.2	2115.8	2115.2	2072.0	2095.4	2089.8	2086.6	2118.7[c]
	E_g	2008.2 (2002.2)	2015.5	2028.5	2028.9	1981.3	2006.1	2000.6	1998.3	2026.7[c]
	T_{1u}	1988.5 (1982.9)	1994.0	2006.8	2007.2	1962.1	1985.2	1979.8	1977.2	1999[d]

[a] The molecular structure is depicted in Figure 1. [b] Reference 41 and 43. [c] Reference 105. [d] Reference 70.

TABLE 2: Geometrical Parameters (Lengths in Å, Angles in Deg), Scaled C−O Stretching Vibrational Frequencies (cm^{-1}), and Dipole Moment (Debye) of the C_{4v} ($^1A_1$) Structure of Cr(CO)$_5$ from DFT Calculations Using the 6-311+G(3df) Basis Set (in Parentheses, Calculated Results Using the 6-311+G(d) Basis Set)

$^1A_1$		hybrid				GGA				exp
		B3LYP	B3PW91	B3P86	mPW1PW91	BLYP	BPW91	BP86	PBE	
geom[a]	r(Cr−C$_{ax}$)	1.853 (1.855)	1.830	1.826	1.830	1.852	1.826	1.828	1.822	
	r(C$_{ax}$−O$_{ax}$)	1.146 (1.149)	1.146	1.145	1.143	1.161	1.160	1.161	1.161	
	r(Cr−C$_{eq}$)	1.926 (1.927)	1.905	1.901	1.903	1.932	1.906	1.907	1.903	
	r(C$_{eq}$−O$_{eq}$)	1.140 (1.143)	1.140	1.139	1.137	1.155	1.154	1.155	1.154	
	∠C$_{ax}$CrC$_{eq}$	90.80 (90.87)	89.88	89.86	89.75	90.93	89.75	89.87	89.38	
	∠C$_{eq}$CrC$_{eq}$	89.99 (89.99)	90.00	90.00	90.00	89.98	90.00	90.00	89.99	
	∠CrC$_{eq}$O$_{eq}$	178.15 (178.20)	177.19	177.22	177.01	178.40	177.13	177.29	176.69	
freq	A_1	2076.3 (2071.8)	2081.6	2095.1	2095.6	2047.5	2070.4	2064.7	2061.2	
	B_2	1995.5 (1989.4)	2002.3	2015.4	2016.4	1964.9	1988.9	1983.4	1980.7	
	E	1972.0 (1966.4)	1976.3	1989.1	1990.4	1940.8	1962.5	1957.2	1954.1	1980,[b] 1976[c]
	A_1	1950.6 (1945.8)	1955.9	1968.4	1969.2	1923.4	1947.9	1942.3	1939.5	1948,[b] 1950[c]
μ		2.204 (2.241)	2.263	2.263	2.280	2.141	2.202	2.185	2.218	

[a] The molecular structure is depicted in Figure 2. [b] Reference 46. [c] Reference 70.

TABLE 3: Geometrical Parameters (Lengths in Å, Angles in Deg), Scaled C−O Stretching Vibrational Frequencies (cm^{-1}), $\langle S^2 \rangle$, and Relative Energies (kcal/mol) of the D_{3h} ($^3A_1'$) Structure of Cr(CO)$_5$ from DFT Calculations Using the 6-311+G(3df) Basis Set (in Parentheses, Calculated Results Using the 6-311+G(d) Basis Set)

$^3A_1'$		hybrid				GGA			
		B3LYP	B3PW91	B3P86	mPW1PW91	BLYP	BPW91	BP86	PBE
geom[a]	r(Cr−C$_{ax}$)	1.921 (1.923)	1.900	1.896	1.899	1.927	1.901	1.902	1.898
	r(C$_{ax}$−O$_{ax}$)	1.141 (1.144)	1.141	1.140	1.138	1.156	1.155	1.156	1.155
	r(Cr−C$_{eq}$)	1.954 (1.956)	1.932	1.927	1.932	1.952	1.924	1.924	1.920
	r(C$_{eq}$−O$_{eq}$)	1.138 (1.141)	1.138	1.137	1.135	1.154	1.152	1.153	1.153
freq	A$_1'$	2070.1 (2065.3)	2074.5	2087.7	2089.3	2036.6	2058.3	2052.6	2048.8
	E$'$	1990.6 (1984.3)	1996.2	2008.8	2010.9	1955.5	1978.6	1973.1	1969.9
	A$_1'$	1980.6 (1974.8)	1987.0	2000.0	2001.5	1947.3	1970.9	1965.6	1962.7
	A$_2''$	1962.1 (1957.0)	1966.3	1979.6	1978.9	1935.8	1957.1	1952.1	1948.9
$\langle S^2 \rangle$		2.038 (2.039)	2.034	2.031	2.043	2.017	2.016	2.014	2.015
ΔE_{rel}[b]		11.2 (11.6)	12.4	12.8	11.5	14.2	15.8	15.6	16.1
ΔH_{rel}[c]		10.6 (10.9)	11.7	12.1	10.8	13.5	15.1	14.9	15.4

[a] The molecular structure is depicted in Figure 2. [b] $\Delta E_{rel} = E(^3A_1') - E(^1A_1)$. [c] $\Delta H_{rel} = H(^3A_1') - H(^1A_1)$.

TABLE 4: Geometrical Parameters (Lengths in Å, Angles in Deg), Scaled C−O Stretching Vibrational Frequencies (cm^{-1}), Dipole Moment (Debye), $\langle S^2 \rangle$, and Relative Energies (kcal/mol) of the C_{2v} ($^1A_1$ and $^3B_2$) and D_{2d} ($^5B_2$) Structures of Cr(CO)$_4$ from DFT Calculations Using the 6-311+G(3df) Basis Set (in Parentheses, Calculated Results Using the 6-311+G(d) Basis Set)

		hybrid				GGA				
		B3LYP	B3PW91	B3P86	mPW1PW91	BLYP	BPW91	BP86	PBE	exp
$^1A_1$ geom[a]	r(Cr−C$_A$)	1.923 (1.924)	1.901	1.898	1.900	1.927	1.901	1.902	1.897	
	r(C$_A$−O$_A$)	1.142 (1.145)	1.142	1.141	1.139	1.157	1.156	1.157	1.157	
	r(Cr−C$_B$)	1.842 (1.843)	1.818	1.815	1.819	1.838	1.812	1.813	1.807	
	r(C$_B$−O$_B$)	1.149 (1.152)	1.149	1.148	1.146	1.165	1.164	1.165	1.165	
	∠C$_A$CrC$_A$	180.06 (180.00)	183.63	183.81	184.08	179.55	184.07	183.83	185.42	
	∠C$_B$CrC$_B$	91.25 (91.36)	90.13	90.08	90.07	90.94	89.64	89.77	89.22	
	∠C$_A$CrC$_B$	89.98 (90.00)	88.72	88.65	88.57	90.16	88.56	88.64	88.07	
	∠CrC$_A$O$_A$	176.25 (176.22)	174.62	174.59	174.33	176.71	174.61	174.77	173.88	
	∠CrC$_B$O$_B$	179.86 (179.89)	179.54	179.56	179.43	179.89	179.60	179.68	179.37	
freq	A$_1$	2048.4 (2043.8)	2053.4	2066.6	2067.7	2015.5	2038.6	2032.7	2029.3	
	B$_2$	1955.0 (1949.6)	1958.4	1971.0	1972.8	1919.5	1940.0	1934.6	1931.1	1957,[b] 1954[c]
	A$_1$	1944.6 (1939.4)	1950.4	1962.8	1964.1	1912.8	1937.3	1931.6	1928.7	
	B$_1$	1920.7 (1915.8)	1926.2	1938.4	1939.7	1889.2	1914.5	1908.8	1906.3	1920,[b] 1916[c]
μ		3.738 (3.790)	3.861	3.864	3.874	3.709	3.835	3.813	3.858	
$^3B_2$ geom[a]	r(Cr−C$_A$)	1.925 (1.926)	1.906	1.902	1.906	1.926	1.903	1.904	1.901	
	r(C$_A$−O$_A$)	1.144 (1.147)	1.144	1.143	1.141	1.159	1.158	1.159	1.158	
	r(Cr−C$_B$)	1.954 (1.954)	1.930	1.924	1.933	1.942	1.915	1.915	1.910	
	r(C$_B$−O$_B$)	1.140 (1.143)	1.140	1.139	1.137	1.156	1.155	1.156	1.156	
	∠C$_A$CrC$_A$	171.12 (171.29)	173.62	173.69	173.91	170.63	173.82	173.33	174.60	
	∠C$_B$CrC$_B$	131.33 (130.30)	129.70	129.15	130.68	127.68	126.39	126.17	125.65	
	∠C$_A$CrC$_B$	91.83 (91.83)	91.35	91.35	91.27	92.06	91.39	91.51	91.23	
	∠CrC$_A$O$_A$	178.78 (178.82)	179.91	179.88	179.99	178.39	179.89	179.57	179.68	
	∠CrC$_B$O$_B$	173.63 (173.33)	173.64	173.60	173.75	173.15	173.07	173.22	172.92	
freq	A$_1$	2052.8 (2047.7)	2056.0	2069.0	2071.0	2017.3	2037.9	2033.1	2028.2	
	B$_2$	1977.3 (1971.9)	1979.5	1991.4	1994.2	1941.6	1961.3	1957.1	1952.4	
	A$_1$	1960.7 (1954.2)	1965.7	1978.7	1979.6	1927.6	1949.4	1945.1	1940.8	
	B$_1$	1930.6 (1924.1)	1934.9	1949.3	1944.5	1906.7	1927.8	1923.9	1919.8	
μ		1.186 (1.243)	1.323	1.345	1.287	1.329	1.470	1.444	1.503	
$\langle S^2 \rangle$		2.067 (2.070)	2.063	2.055	2.081	2.028	2.027	2.025	2.027	
ΔE_{rel}[d]		7.1 (7.3)	8.9	9.6	7.7	11.5	14.1	14.0	14.7	
ΔH_{rel}[e]		6.5 (6.7)	8.2	8.9	7.0	11.0	13.4	13.4	14.1	
$^5B_2$ geom[a]	r(Cr−C)	1.989 (1.992)	1.969	1.963	1.969	1.983	1.959	1.957	1.955	
	r(C−O)	1.140 (1.143)	1.139	1.138	1.136	1.155	1.153	1.155	1.154	
	∠CCrC	145.12 (145.58)	149.12	148.16	153.50	135.20	139.16	137.92	139.20	
	∠C$_A$CrC$_B$	95.15 (95.02)	94.06	94.32	93.01	98.35	96.99	97.41	96.98	
	∠CrCO	174.44 (174.02)	174.45	174.57	174.47	175.71	175.47	175.63	175.45	
freq	A$_1$	2054.2 (2048.6)	2059.4	2072.4	2074.9	2015.0	2035.4	2029.1	2025.3	
	B$_2$	1969.9 (1962.9)	1976.0	1989.2	1987.8	1938.6	1960.6	1955.0	1951.7	
	E	1968.2 (1961.5)	1975.4	1988.2	1989.1	1938.3	1960.3	1954.5	1951.3	
$\langle S^2 \rangle$		6.071 (6.075)	6.070	6.063	6.085	6.035	6.035	6.032	6.034	
ΔE_{rel}[f]		8.7 (8.9)	9.7	11.6	6.4	19.5	22.1	22.5	23.3	
ΔH_{rel}[g]		7.7 (7.8)	8.6	10.5	5.3	18.5	20.9	21.4	22.2	

[a] The molecular structures are depicted in Figure 3. [b] Reference 46. [c] Reference 70. [d] $\Delta E_{rel} = E(^3B_2) - E(^1A_1)$. [e] $\Delta H_{rel} = H(^3B_2) - H(^1A_1)$. [f] $\Delta E_{rel} = E(^5B_2) - E(^1A_1)$. [g] $\Delta H_{rel} = H(^5B_2) - H(^1A_1)$.

appropriate method. The results are summarized in Table 1S in the Supporting Information.

For Cr(CO)$_2$ and Cr(CO)$_3$, where the discrepancy between our DFT calculations and previously reported results was found,

we performed additional ab initio calculations such as MP2,[85,86] CCSD,[87,88] and CCSD(T)[89] (for Cr(CO)$_2$ only) with the 6-311+G-(d) basis set for selected molecules. Due to the computational cost, we used the 6-311+G(d) basis set for ab initio calculations.

TABLE 5: Geometrical Parameters (Lengths in Å, Angles in Deg), Scaled C−O Stretching Vibrational Frequencies (cm⁻¹), Dipole Moment (Debye), $\langle S^2 \rangle$, and Relative Energies (kcal/mol) of the D_{4h} ($^1A_{1g}$) and D_{2h} ($^3B_{1g}$) Structures of Cr(CO)4 from DFT Calculations Using the 6-311+G(3df) Basis Set (in Parentheses, Calculated Results Using the 6-311+G(d) Basis Set)

			hybrid				GGA			
			B3LYP	B3PW91	B3P86	mPW1PW91	BLYP	BPW91	BP86	PBE
$^1A_{1g}$	geom[a]	r(Cr−C)	1.921 (1.922)	1.902	1.898	1.900	1.924	1.900	1.901	1.897
		r(C−O)	1.143 (1.146)	1.143	1.142	1.140	1.159	1.157	1.158	1.158
	freq	A_{1g}	2056.2 (2051.2)	2060.2	2073.4	2074.8	2025.4	2047.5	2042.1	2038.3
		B_{1g}	1972.5 (1966.3)	1978.9	1991.8	1992.5	1945.1	1969.7	1964.4	1961.8
		E_u	1945.1 (1939.4)	1947.5	1960.1	1961.9	1913.5	1933.8	1928.9	1925.4
	ΔE_{rel}[b]		10.7 (10.6)	13.3	13.6	12.9	13.5	16.8	16.6	17.8
	ΔH_{rel}[c]		10.5 (10.4)	13.0	13.3	12.6	13.3	16.5	16.4	17.5
$^3B_{1g}$	geom[a]	r(Cr−C)	1.954 (1.955)	1.935	1.930	1.935	1.954	1.931	1.931	1.928
		r(C−O)	1.141 (1.144)	1.141	1.140	1.138	1.156	1.155	1.156	1.155
		∠CCrC	97.08 (96.98)	97.74	97.74	97.99	96.74	97.55	97.47	97.97
		∠CrCO	177.95 (177.99)	177.70	177.69	177.56	178.14	177.92	177.92	177.66
	freq	A_g	2062.9 (2057.6)	2067.0	2080.6	2081.0	2033.5	2054.2	2049.1	2044.7
		B_{2u}	1960.4 (1954.0)	1963.8	1977.0	1977.9	1928.6	1948.6	1944.1	1939.9
		B_{1u}	1948.6 (1941.9)	1950.7	1965.3	1960.6	1924.4	1943.5	1939.4	1935.2
		B_{3g}	1877.9 (1871.3)	1887.0	1902.3	1895.7	1872.5	1896.5	1893.2	1892.2
	$\langle S^2 \rangle$		2.074 (2.078)	2.071	2.063	2.086	2.036	2.036	2.033	2.037
	ΔE_{rel}[d]		7.9 (8.0)	9.9	10.7	8.4	13.6	16.6	16.5	17.3
	ΔH_{rel}[d]		7.1 (7.3)	9.1	9.9	7.5	12.3	15.7	15.7	16.4

[a] The molecular structures are depicted in Figure 3. [b] $\Delta E_{rel} = E(^1A_{1g}) - E(^1A_1)$. [c] $\Delta H_{rel} = H(^1A_{1g}) - H(^1A_1)$. [d] $\Delta E_{rel} = E(^3B_{1g}) - E(^1A_1)$. [e] $\Delta H_{rel} = H(^3B_{1g}) - H(^1A_1)$.

In addition, we calculated these molecules again using various DFT functionals with the 6-311+G(d) basis set to compare the results with those of ab initio calculation. All ab initio calculations were performed with the frozen core approximation. We performed the geometry optimization and calculated vibrational frequencies with all methods employed in this work.

For presenting the vibrational frequencies, we used scale factors listed on the web page of the National Institute of Standards and Technology:[90] 0.961, 0.957, 0.954, 0.995, and 0.990 for B3LYP, B3PW91, mPW1PW91, BLYP, and PBE, respectively. There are no scale factors available for B3P86, BPW91, and BP86. Because B3P86 is hybrid functional, we used the scale factor (0.961) of B3LYP, which is also hybrid functional as B3P86. For the same reason, for BPW91 and BP86, which are GGA functionals, we used 0.995, which is originally the scale factor of BLYP. In the ab initio calculations, we used 0.950, 0.954, and 0.963 for Möller−Plesset second order (MP2), CCSD, and CCSD(T), respectively.

To clarify the bonding nature between chromium and the carbonyl groups, we performed NBO analysis,[91] which can aid the interpretation of the metal−ligand interaction in terms of the second-order perturbative energies. In addition, the NBO results contain the natural electron configuration of Cr atom. The NBO analysis is performed only at the optimized structure using B3LYP/6-311+G(d). The results of NBO analysis and the charges of all species are summarized in the Supporting Information.

Results and Discussion

A. Molecular Structures. *1. Cr(CO)₆.* The fully optimized structure of Cr(CO)₆ with O_h symmetry is summarized in Figure 1 and Table 1. In previous studies, the geometry of Cr-(CO)₆ was investigated by neutron[41,43] and X-ray diffraction.[40,43] Because X-ray diffraction data have greater uncertainty, we used neutron diffraction data: 1.918 Å for r_e(Cr−C) and 1.141 Å for r_e(C−O) including a thermal correction for measurements taken at 78 K. As shown in Table 1, the results from all functionals except B3LYP and BLYP underestimate the Cr−C distance compared to the experimental value. The calculation using B3LYP gives a slightly larger Cr−C distance (1.926 Å)
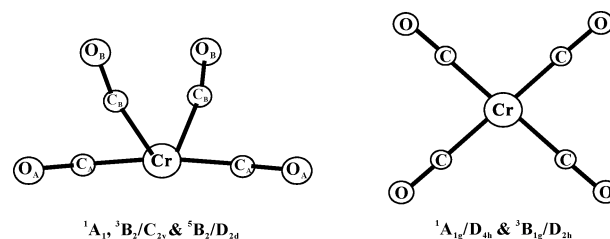

Figure 3. Molecular structures of Cr(CO)₄ (molecular state/molecular symmetry).

compared with the experimental value (1.918 Å). Calculations using B3LYP and the BLYP functionals give a longer Cr−C distance compared with other functionals. In the C−O bond length, all calculations using hybrid functionals provide reasonable bond lengths. However, all GGA functionals overestimate the C−O bond length compared with the experimental value. In the case of the geometry of Cr(CO)₆, the B3LYP gives good results. Compared with the result using 6-311+G(3df) basis set, the calculated bond lengths using the 6-311+G(d) basis set is slightly longer.

In the case of the C−O stretching frequency, all hybrid functionals show better performance than all GGA functionals which underestimate the C−O stretching frequency. The calculated frequencies using B3P86 and mPW1PW91 are in excellent agreement with experimental values. The B3LYP functional gives reasonable geometries but slightly underestimates the stretching frequencies.

In the natural population analysis (NPA), hybrid functionals generally give larger charges than those of GGA functionals (See Table 2S in Supporting Information). The B3LYP and the BLYP functionals give small charges compared with other functionals.

2. Cr(CO)₅. Cr(CO)₅ can adopt two different symmetries and its optimized structures are depicted in Figure 2. Experimentally, the matrix-isolated Cr(CO)₅ was shown to have C_{4v} symmetry where the ∠C_{ax}−Cr−C_{eq} angle is approximately between 90° and 95°[92] although the D_{3h} structure had also been proposed under certain conditions.[93] Although there is no available gas-phase experimental structural information, several theoretical studies of Cr(CO)₅ were performed by ab initio[23,28,57,94] and DFT

TABLE 6: Geometrical Parameters (Lengths in Å, Angles in Deg), Scaled C−O Stretching Vibrational Frequencies (cm⁻¹), Dipole Moment (Debye), ⟨S²⟩, Number of Imaginary Frequencies, and Relative Energies (kcal/mol) of the C_{2v} (¹A₁, ³B₁, and ⁵B₂) Structures of Cr(CO)₃ from DFT Calculations Using the 6-311+G(3df) Basis Set (in Parentheses, Calculated Results Using the 6-311+G(d) Basis Set)

			hybrid				GGA		
			B3LYP	B3PW91	B3P86	mPW1PW91	BLYP	BPW91	BP86	PBE
¹A₁	geom[a]	$r(Cr-C_A)$	1.823 (1.824)	1.798	1.795	1.800	1.816	1.790	1.791	1.786
		$r(C_A-O_A)$	1.155 (1.158)	1.155	1.155	1.152	1.172	1.171	1.172	1.172
		$r(Cr-C_B)$	1.916 (1.917)	1.895	1.892	1.895	1.917	1.893	1.894	1.889
		$r(C_B-O_B)$	1.146 (1.149)	1.146	1.145	1.143	1.162	1.162	1.162	1.162
		$\angle C_B Cr C_B$	181.63 (181.49)	185.61	185.85	185.97	181.54	186.47	186.28	187.89
		$\angle C_A Cr C_B$	89.19 (89.25)	87.19	87.08	87.01	89.23	86.76	86.86	86.01
		$\angle Cr C_B O_B$	176.52 (176.57)	174.76	174.69	174.46	176.75	174.66	174.76	173.93
	freq	A₁	2019.9 (2014.7)	2024.1	2037.2	2039.6	1984.0	2004.9	1999.6	1995.8
		B₂	1922.6 (1916.8)	1925.5	1938.1	1940.6	1886.0	1905.1	1900.4	1896.7
		A₁	1898.6 (1893.2)	1902.0	1914.2	1916.0	1868.6	1890.1	1885.1	1882.9
	μ		3.568 (3.611)	3.786	3.792	3.784	3.618	3.853	3.831	3.884
	ΔE_{rel}[b]		15.5 (15.5)	16.8	14.7	20.1	4.8	5.3	4.3	4.7
	ΔH_{rel}[c]		16.2 (16.2)	17.6	15.5	20.9	6.1	6.9	5.6	6.1
³B₁	geom[a]	$r(Cr-C_A)$	1.919 (1.921)	1.896	1.889	1.900	1.902	1.876	1.876	1.871
		$r(C_A-O_A)$	1.142 (1.145)	1.142	1.141	1.139	1.158	1.157	1.158	1.158
		$r(Cr-C_B)$	1.921 (1.921)	1.903	1.899	1.904	1.920	1.899	1.899	1.896
		$r(C_B-O_B)$	1.149 (1.152)	1.149	1.148	1.146	1.164	1.163	1.164	1.164
		$\angle C_B Cr C_B$	176.29 (176.25)	178.58	178.80	178.76	176.36	179.29	179.18	179.96
		$\angle C_A Cr C_B$	91.86 (91.87)	90.71	90.60	90.62	91.82	90.36	90.41	89.98
		$\angle Cr C_B O_B$	178.90 (178.98)	177.71	177.67	177.49	179.09	177.65	177.74	177.21
	freq	A₁	2025.0 (2019.5)	2029.0	2042.0	2043.9	1990.4	2012.3	2006.5	2002.8
		A₁	1947.0 (1940.7)	1951.6	1964.3	1964.8	1916.8	1938.7	1933.2	1929.8
		B₂	1888.3 (1881.1)	1890.5	1906.6	1893.6	1870.1	1890.3	1886.5	1881.9
	μ		1.989 (2.017)	2.101	2.121	2.096	2.034	2.156	2.141	2.175
	⟨S²⟩		2.091 (2.095)	2.088	2.078	2.112	2.041	2.040	2.037	2.040
	imag freq		0	0	0	0	1	1	1	1
	ΔE_{rel}[d]		6.4 (6.6)	6.9	5.6	9.0	−1.2	−1.2	−2.0	−1.7
	ΔH_{rel}[e]		6.9 (7.0)	7.4	6.1	9.5	−0.69	−0.71	−1.5	−1.2
⁵B₂	geom[a]	$r(Cr-C_A)$	1.984	1.965	1.956	1.968	1.972	1.948	1.946	1.944
		$r(C_A-O_A)$	1.144	1.144	1.143	1.142	1.158	1.157	1.158	1.158
		$r(Cr-C_B)$	1.997	1.982	1.975	1.984	1.994	1.975	1.973	1.972
		$r(C_B-O_B)$	1.141	1.140	1.140	1.137	1.156	1.155	1.156	1.155
		$\angle C_B Cr C_B$	153.35	155.20	155.05	155.40	152.91	155.34	154.87	155.55
		$\angle C_A Cr C_B$	103.33	102.40	102.47	102.30	103.55	102.33	102.56	102.22
		$\angle Cr C_B O_B$	178.83	178.20	178.30	177.96	179.40	178.53	178.79	178.34
	freq	A₁	2037.4	2041.9	2054.7	2057.1	2001.5	2023.5	2017.4	2013.9
		B₂	1956.3	1962.8	1975.5	1976.6	1925.6	1948.9	1943.3	1940.5
		A₁	1943.4	1948.8	1963.0	1957.5	1922.1	1945.0	1939.3	1936.7
	μ		0.938	0.909	0.888	0.973	0.829	0.801	0.789	0.808
	⟨S²⟩		6.104	6.106	6.093	6.129	6.052	6.053	6.048	6.052
	imag freq		0	0	0	0	1	1	1	1

[a] The molecular structures are depicted in Figure 4. [b] $\Delta E_{rel} = E(^1A_1) - E(^5B_2)$. [c] $\Delta H_{rel} = H(^1A_1) - H(^5B_2)$. [d] $\Delta E_{rel} = E(^3B_1) - E(^5B_2)$. [e] $\Delta H_{rel} = H(^3B_1) - H(^5B_2)$.

methods.[35] Previous studies showed that the C_{4v} structure is more stable than the D_{3h} structure and the energy difference between two symmetries are 9−10 kcal/mol[57,94] at the Hartree−Fock (HF) level with small basis sets. Our calculations confirm that the C_{4v} structure (¹A₁) is more stable than the D_{3h} (³A′₁) one for all DFT functionals (see Table 3). The energy differences between these two states using GGA functionals are larger than those from using hybrid functionals. Other Cr(CO)ₙ species (n = 1−4) also show such trend (see other sections).

We now consider the bond lengths shown in Tables 2 and 3. Both the hybrid and GGA functionals except the B3LYP and the BLYP provide similar Cr−C distances. The results with the B3LYP and BLYP functionals show significantly longer Cr−C distances compared with those with other functionals. This trend was also observed for Cr(CO)₆. All calculations using GGA functionals give longer C−O bond lengths compared with hybrid functionals, as in the Cr(CO)₆ case. The equatorial metal−ligand (Cr−C) bond lengths of both the C_{4v} and D_{3h} structure are longer than the axial Cr−C bond lengths. In contrast, the equatorial C−O bond lengths of both structures are shorter than the axial ones. These indicate that the bonding interaction between the

axial C−O ligand and the Cr atom is stronger than that between the equatorial ligand and Cr and can be explained by considering the increased occupation of π^* orbital in C−O because the bonding interaction between Cr and C−O is proportional to the occupation of π^* orbital in C−O through π back-bonding. The results of the NBO analysis at the B3LYP/6-311+G(d) level show that the occupation number of π^* orbital at axial C−O (¹A₁, 0.37516; ³A′₁, 0.32865) is larger than that (¹A₁, 0.27683; ³A′₁, 0.28239) at equatorial C−O. The increased occupation of π^* orbital also reduces the stretching frequency of C−O.[95] As shown in Tables 2 and 3, the stretching frequencies of axial C−O of both structures (¹A₁, ³A′₁) are smaller than those of equatorial C−O (¹A₁:A₁ < B₂, E and ³A₁′:A₂″ < E′).

Calculations using only the B3LYP and BLYP functionals provide $\angle C_{ax}-Cr-C_{eq}$ angles that fall within the range of experimental data. Previous theoretical calculations gave similar results.[23,35] However, the MP2 method gives a rather different result that $\angle C_{ax} Cr C_{eq}$ is smaller than 90°.[28] All functionals except B3LYP and BLYP provide results similar to the MP2 result. The geometry optimization with B3LYP/6-311+G(3df) produces results similar to B3LYP/6-311+G(d) calculations for

TABLE 7: Geometrical Parameters (Lengths in Å, Angles in Deg), Scaled C−O Stretching Vibrational Frequencies (cm⁻¹), Dipole Moment (Debye), ⟨S²⟩, and Relative Energies (kcal/mol) of the C_{3v} (¹A₁) and D_{3h} (⁷A₂″) Structures of Cr(CO)₃ from DFT Calculations Using the 6-311+G(3df) Basis Set (in Parentheses, Calculated Results Using the 6-311+G(d) Basis Set)

			hybrid				GGA				
			B3LYP	B3PW91	B3P86	mPW1PW91	BLYP	BPW91	BP86	PBE	exp
¹A₁	geom[a]	r(Cr−C)	1.827	1.803	1.799	1.804	1.820	1.793	1.795	1.789	
		r(C−O)	1.153	1.153	1.152	1.150	1.170	1.169	1.170	1.170	
		∠CCrC	90.25	88.69	88.60	88.56	90.25	88.31	88.43	87.72	
		∠CrCO	178.79	178.32	178.35	178.07	179.37	178.78	178.79	178.42	
	freq	A₁	1986.6	1990.7	2003.4	2005.8	1949.3	1973.1	1967.2	1963.8	
		E	1893.4	1897.8	1909.9	1912.2	1856.1	1879.3	1873.8	1870.2	1880,[b] 1887[c]
	μ		5.548	5.752	5.755	5.751	5.580	5.802	5.774	5.830	
	ΔE_{rel}[d]		3.7	2.4	−0.066	6.1	−10.1	−13.0	−14.0	−14.7	
	ΔH_{rel}[e]		4.7	3.5	1.1	7.3	−8.5	−11.3	−12.3	−12.9	
⁷A₂	geom[a]	r(Cr−C)	2.055 (2.058)	2.039	2.030	2.041	2.043	2.022	2.018	2.017	
		r(C−O)	1.141 (1.144)	1.140	1.139	1.136	1.157	1.155	1.156	1.155	
	freq	A₁′	2026.6 (2020.2)	2034.1	2046.6	2050.1	1985.9	2010.9	2004.8	2001.4	
		E′	1951.6 (1943.5)	1964.0	1976.2	1976.7	1924.1	1953.6	1948.2	1945.5	
	⟨S²⟩		12.010 (12.010)	12.014	12.013	12.015	12.007	12.010	12.009	12.009	
	ΔE_{rel}[f]		6.6 (7.0)	4.9	6.2	2.9	14.4	12.5	13.6	13.1	
	ΔH_{rel}[g]		6.4 (6.7)	4.6	6.0	2.7	14.8	12.9	14.0	13.5	

[a] The molecular structures are depicted in Figure 4. [b] Reference 46. [c] Reference 70. [d] $\Delta E_{rel} = E(^1A_1) - E(^5B_2)$. [e] $\Delta H_{rel} = H(^1A_1) - H(^5B_2)$. [f] $\Delta E_{rel} = E(^7A_2'') - E(^5B_2)$. [g] $\Delta H_{rel} = H(^7A_2'') - H(^5B_2)$.

TABLE 8: Geometrical Parameters[a] (Lengths in Å, Angles in Deg), Stretching Vibrational Frequencies[b] of C−O (cm⁻¹), Dipole Moment (Debye), ⟨S²⟩, Number of Imaginary Frequencies, and Relative Energies (kcal/mol) between the C_{2v} (⁵B₂) and C_{3v} (¹A₁) Structures of Cr(CO)₃ from Calculations Using the 6-311+G(d) Basis Set (in Parentheses, Results of Single Point Calculation Using the 6-311+G(3df) Basis Set at Optimized Geometry Using the 6-311+G(d) Basis Set)

6-311+G(d)	B3LYP	B3PW91	B3P86	mPW1PW91	BLYP	BPW91	BP86	PBE	MP2	CCSD
					C_{2v} (⁵B₂)						
r(Cr−C_A)	1.985	1.967	1.958	1.970	1.973	1.950	1.947	1.946	2.033	2.000
r(C_A−O_A)	1.148	1.147	1.146	1.145	1.162	1.160	1.161	1.161	1.136	1.150
r(Cr−C_B)	1.999	1.984	1.977	1.986	1.995	1.976	1.974	1.973	1.979	2.026
r(C_B−O_B)	1.144	1.143	1.143	1.140	1.160	1.158	1.159	1.159	1.159	1.140
∠C_BCrC_B	153.94	155.58	155.41	155.46	153.57	155.65	155.42	155.55	159.83	152.62
∠C_ACrC_B	103.03	102.21	102.30	102.27	103.22	102.17	102.29	102.22	100.08	103.69
∠CrC_BO_B	178.47	177.82	177.94	177.75	179.01	178.21	178.35	178.23	173.57	177.96
A₁	2113.6	2030.3	2036.2	2046.8	1922.5	1947.5	1941.9	1949.0	1666.4	1970.1
B₂	2028.7	2045.2	2049.4	2067.3	1926.0	1951.6	1945.5	1952.8	2020.0	2079.3
A₁	2013.1	2129.1	2133.0	2153.1	2003.1	2027.4	2021.0	2028.0	2123.5	2155.4
μ	0.976	0.945	0.927	1.007	0.863	0.834	0.824	0.833	2.847	1.382
⟨S²⟩	6.109	6.110	6.097	6.134	6.053	6.055	6.050	6.054	6.707	6.752 (6.760)
imag freq	0	0	0	0	1	1	1	1	1	0
					C_{3v} (¹A₁)						
r(Cr−C)	1.828	1.804	1.800	1.805	1.821	1.795	1.796	1.791	1.740	1.844
r(C−O)	1.156	1.156	1.155	1.153	1.173	1.172	1.173	1.173	1.179	1.154
∠CCrC	90.35	88.93	88.86	88.84	90.28	88.59	88.70	87.95	87.15	88.58
∠CrCO	178.91	178.51	178.52	178.24	179.42	178.93	179.17	178.42	177.26	177.36
A₁	2063.2	2077.5	2081.3	2100.4	1951.4	1978.9	1974.3	1980.3	1997.6	2100.5
E	1965.4	1979.6	1983.3	2001.4	1857.0	1884.2	1880.2	1885.4	1928.2	1976.6
μ	5.611	5.791	5.795	5.787	5.655	5.838	5.804	5.862	6.408	5.629
ΔE_{rel}[c]	3.8	2.5	0.092	6.3	−10.3	−13.1	−14.1	−14.7	−51.8	18.5 (13.0)
ΔH_{rel}[d]	4.8	3.6	1.2	7.4	−8.7	−11.4	−12.3	−13.0	−48.8	19.5

[a] The molecular structures are depicted in Figure 4. [b] Unscaled value. [c] $\Delta E_{rel} = E(^1A_1) - E(^5B_2)$. [d] $\Delta H_{rel} = H(^1A_1) - H(^5B_2)$.

both C_{4v} and D_{3h} structures. Compared with the 6-311+G(d) basis set, both bond lengths and angles of the 6-311+G(3df) basis set are slightly reduced, but the basis set dependency is small in DFT calculations, showing essentially the same trend as in the case of Cr(CO)₆.

All results with GGA functionals underestimate the C−O stretching frequency, and the hybrid functionals show better performance. Especially, the results of B3LYP and B3PW91 are in good agreement with experimental values. In summary, according to the results of Cr(CO)₆ and Cr(CO)₅, both hybrid and GGA functionals give similar results for Cr−C bond lengths except those based on the LYP functional. However, for C−O bond lengths, the hybrid functionals give better results. In general, the GGA functionals overestimate the bond length of C−O. For C−O stretching frequencies, the hybrid functionals

give good results whereas the calculations using GGA functionals underestimate the C−O stretching frequency. Because this trend in geometries and frequencies between the hybrid and the GGA functionals are the same in all other Cr(CO)ₙ, we will omit comments about these trends in other cases following.

We summarize the results of NBO analysis on the interaction between the d orbital of the Cr atom and the antibonding orbital of CO in Table 4S (Supporting Information). The NBO results clearly show the back-donation of metal. The back-donations to axial COs are larger than those of equatorial ones in each species. Actually, it is expected that the removal of the opposing "axial" CO group in Cr(CO)₆ results in reinforcing electron density into the remaining axial bonding orbital. The NPA charges confirm these explanations (see Tables 2S and 3S in Supporting Information). In the C_{4v} structure, the atoms of axial

TABLE 9: Geometrical Parameters (Lengths in Å, Angles in Deg), Scaled C−O Stretching Vibrational Frequencies (cm^{-1}), Dipole Moment (Debye), $\langle S^2 \rangle$, and Relative Energies (kcal/mol) of Linear Structures ($^1\Sigma_g$, $^3\Sigma_g$, $^5\Pi_g$, $^7\Pi_u$, and $^9\Sigma_u$) of Cr(CO)$_2$ from DFT Calculations Using the 6-311+G(3df) Basis Set (in Parentheses, Calculated Results Using the 6-311+G(d) Basis Set)

			hybrid				GGA		
			B3LYP	B3PW91	B3P86	mPW1PW91	BLYP	BPW91	BP86	PBE
$^1\Sigma_g$	geom^a	r(Cr−C)	1.911 (1.911)	1.896	1.892	1.895	1.921	1.901	1.901	1.898
		r(C−O)	1.153 (1.157)	1.153	1.152	1.150	1.175	1.174	1.175	1.174
	freq	Σ_g	1978.0 (1971.0)	1982.5	1996.1	1996.9	1881.8	1899.9	1897.0	1892.9
		Σ_u	1875.9 (1868.4)	1878.1	1891.2	1891.1	1823.3	1841.7	1838.3	1834.0
	$\Delta E_{\text{rel}}{}^b$		42.1 (42.0)	49.8	46.1	54.9	153.1	161.3	157.6	159.8
	$\Delta H_{\text{rel}}{}^c$		42.7 (42.6)	50.4	46.7	55.5	153.5	161.8	158.1	160.3
$^3\Sigma_g$	geom^a	r(Cr−C)	1.919 (1.919)	1.904	1.900	1.905	1.917	1.899	1.899	1.896
		r(C−O)	1.156 (1.159)	1.155	1.154	1.152	1.171	1.170	1.171	1.171
	freq	Σ_g	1968.0 (1960.9)	1972.6	1987.2	1986.5	1934.3	1955.3	1951.4	1947.3
		Σ_u	1845.4 (1838.5)	1845.3	1862.1	1848.9	1828.0	1845.1	1842.8	1837.6
	$\langle S^2 \rangle$		2.115 (2.120)	2.116	2.104	2.143	2.057	2.058	2.053	2.059
	$\Delta E_{\text{rel}}{}^d$		16.9 (16.8)	21.4	18.7	25.6	2.1	6.8	4.6	6.2
	$\Delta H_{\text{rel}}{}^e$		17.4 (17.4)	21.9	19.2	26.2	2.6	7.4	5.1	6.7
$^5\Pi_g$	geom^a	r(Cr−C)	1.989	1.977	1.969	1.981	1.981	1.965	1.963	1.963
		r(C−O)	1.147	1.147	1.146	1.144	1.161	1.160	1.161	1.160
	freq	Σ_g	2012.2	2017.3	2031.6	2030.3	1984.8	2007.8	2002.9	1998.8
		Σ_u	1805.7	1779.0	1818.4	1636.1	1882.1	1900.6	1898.6	1893.6
	$\langle S^2 \rangle$		6.184	6.195	6.174	6.235	6.087	6.095	6.084	6.094
	$\Delta E_{\text{rel}}{}^f$		−5.9	−5.1	−5.2	−4.4	−6.1	−5.2	−5.1	−4.7
	$\Delta H_{\text{rel}}{}^g$		−5.4	−4.8	−4.8	−4.3	−5.7	−4.8	−4.7	−4.3
	$\Delta E_{\text{rel}}{}^h$		−2.7	0.21	−1.3	2.8	−12.6	−9.3	−10.9	−9.8
	$\Delta H_{\text{rel}}{}^i$		−2.6	0.23	−1.3	2.5	−12.3	−9.1	−10.7	−9.6
$^7\Pi_u$	geom^a	r(Cr−C)	2.049	2.037	2.029	2.036	2.047	2.031	2.028	2.028
		r(C−O)	1.147	1.146	1.145	1.143	1.162	1.160	1.161	1.160
	freq	Σ_g	1982.5	1990.7	2003.7	2004.2	1953.4	1980.4	1974.9	1972.2
		Σ_u	1913.3	1926.5	1938.4	1936.0	1896.0	1926.6	1921.2	1919.2
	$\langle S^2 \rangle$		12.006	12.009	12.008	12.009	12.004	12.007	12.006	12.006
$^9\Sigma_u$	geom^a	r(Cr−C)	1.958 (1.961)	1.944	1.938	1.938	1.979	1.960	1.958	1.957
		r(C−O)	1.185 (1.189)	1.182	1.181	1.179	1.203	1.199	1.200	1.198
	freq	Σ_u	2345.3 (2332.3)	2192.1	2273.5	2067.6	1269.6	1325.7	1360.6	1375.1
		Σ_g	1750.8 (1739.9)	1775.5	1786.6	1788.5	1723.6	1768.5	1760.3	1763.3
	$\langle S^2 \rangle$		20.006 (20.005)	20.005	20.005	20.006	20.004	20.004	20.004	20.004
	$\Delta E_{\text{rel}}{}^j$		153.9 (154.3)	150.4	151.3	153.9	138.2	134.7	135.7	134.6
	$\Delta H_{\text{rel}}{}^k$		154.4 (154.8)	150.8	151.8	154.1	136.9	133.5	134.5	133.5

^{a} The molecular structures are depicted in Figure 5. ^{b} $\Delta E_{\text{rel}} = E(^1\Sigma_g) - E(^7\Pi_u)$. ^{c} $\Delta H_{\text{rel}} = H(^1\Sigma_g) - H(^7\Pi_u)$. ^{d} $\Delta E_{\text{rel}} = E(^3\Sigma_g) - E(^7\Pi_u)$. ^{e} $\Delta H_{\text{rel}} = H(^3\Sigma_g) - H(^7\Pi_u)$. ^{f} $\Delta E_{\text{rel}} = E(^5\Pi_g) - E(^5A_1)$. ^{g} $\Delta H_{\text{rel}} = H(^5\Pi_g) - H(^5A_1)$. ^{h} $\Delta E_{\text{rel}} = E(^5\Pi_g) - E(^7\Pi_u)$. ^{i} $\Delta H_{\text{rel}} = H(^5\Pi_g) - H(^7\Pi_u)$. ^{j} $\Delta E_{\text{rel}} = E(^9\Sigma_u) - E(^7\Pi_u)$. ^{k} $\Delta H_{\text{rel}} = H(^9\Sigma_u) - H(^7\Pi_u)$.

positions contain more negative charge than those of equatorial positions (see Figure 2). In addition, these charges at axial positions contain more negative charge than those of Cr(CO)$_6$. Therefore, the Cr(CO)$_5$ ($^1A_1$) axial (Cr−C) bond length is shorter than that of the Cr(CO)$_6$ whereas equatorial (Cr−C) bond lengths are similar.

In the $^3A_1{}'$ state, as shown in Table 3, the spin contamination is rather small for all cases, and substantially smaller for GGA than the hybrids.

3. Cr(CO)$_4$. Experimentally, Cr(CO)$_4$ is known to have C_{2v} symmetry in an Ar matrix[96] and a singlet ground state.[97] There are no experimental values or theoretical calculation results for geometrical parameters of Cr(CO)$_4$. The fully optimized structures, relative energies, C−O stretching frequencies and dipole moments of Cr(CO)$_4$ are summarized in Tables 4 and 5 and Figure 3. The results show that the ground state of Cr(CO)$_4$ has a C_{2v} seesaw structure and is a singlet ($^1A_1$). We note that Cr(CO)$_4$ has a higher spin state ($^5B_2$) that is a low-lying excited state.

The geometrical parameters of the seesaw C_{2v} ($^1A_1$) structure are similar to those of the C_{4v} structure of Cr(CO)$_5$ ($^1A_1$) (see Tables 2 and 4). All functionals give similar results. The Cr−C$_A$ and C$_A$−O$_A$ bond length (see Table 4 and Figure 3) of C_{2v} ($^1A_1$) are almost identical to those (Cr−C$_{eq}$ and C$_{eq}$−O$_{eq}$ in Table 2) of Cr(CO)$_5$. The C$_B$−Cr−C$_B$ angle (see Table 4 and Figure 3) of C_{2v} ($^1A_1$) is also equal to that (C$_{ax}$−Cr−C$_{eq}$ in Table 2) of Cr(CO)$_5$. However, all functionals show that the

Cr−C$_B$ bond length of C_{2v} ($^1A_1$) is smaller than the Cr−C$_{ax}$ bond length of Cr(CO)$_5$ and the C$_B$−O$_B$ bond length is larger than C$_{ax}$−O$_{ax}$ of Cr(CO)$_5$. This indicates that the removal of an equatorial CO group from the C_{4v} ($^1A_1$) structure of Cr(CO)$_5$ results in reinforcing the electron density into remaining CO groups. We calculated the BDEs using B3LYP/6-311+G(d) and confirmed these. The BDEs of Cr(CO)$_4$−C$_{ax}$O$_{ax}$ and Cr(CO)$_3$-C$_B$O$_B$ are about 45.5 and 46.3 kcal/mol, respectively. These indicate that the bond strength of Cr−C$_B$ in the C_{2v} ($^1A_1$) structure gets stronger upon the removal of C$_{eq}$O$_{eq}$ from C_{4v} ($^1A_1$) structure.

As shown in Table 4, the C−O stretching frequencies calculated using the B3LYP functional are in excellent agreement with those from the experiment. The B3PW91 and the BPW91 functionals also give good results. The B3P86 and the mPW1PW91 functionals overestimate the frequencies. Spin contaminations are somewhat increased to be compared with those of Cr(CO)$_5$, but still not excessively large. As in the case of Cr(CO)$_5$, spin contaminations are larger for hybrid functionals than for GGA (Tables 4 and 5).

The relative stabilities among several states of Cr(CO)$_4$ can be assigned on the basis of calculated energies and enthalpies as shown in Tables 4 and 5. We note that the results with hybrid and GGA functionals give different orders of energy for the structures. All results with hybrid functionals except the mPW1PW91 functional show the same order of the energy. ($^1A_1$ < $^3B_2$ < $^3B_{1g}$ < $^5B_2$ < $^1A_{1g}$ and $^1A_1$ < $^5B_2$ < $^3B_2$ < $^3B_{1g}$ <
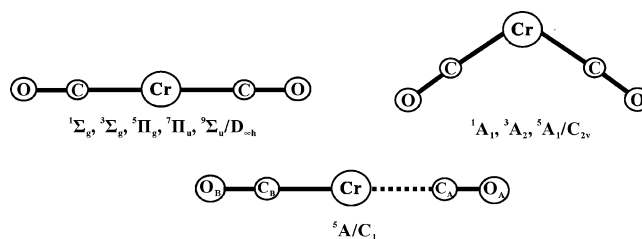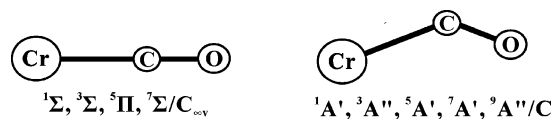
TABLE 10: Geometrical Parameters (Lengths in Å, Angles in Deg), Scaled C−O Stretching Vibrational Frequencies (cm⁻¹), Dipole Moment (Debye), $\langle S^2 \rangle$, and Relative Energies (kcal/mol) of Bent Structures ($^1A_1$, $^3A_2$, and $^5A_1$) of Cr(CO)$_2$ from DFT Calculations Using the 6-311+G(3df) Basis Set (in Parentheses, Calculated Results Using the 6-311+G(d) Basis Set)

			hybrid				GGA				
			B3LYP	B3PW91	B3P86	mPW1PW91	BLYP	BPW91	BP86	PBE	exp
$^1A_1$	geom[a]	r(Cr−C)	1.804 (1.805)	1.782	1.779	1.783	1.797	1.772	1.773	1.768	
		r(C−O)	1.161 (1.164)	1.162	1.161	1.158	1.179	1.179	1.180	1.180	
		∠CCrC	88.29 (88.41)	86.50	86.32	85.92	89.18	87.03	87.02	85.95	
		∠CrCO	178.24 (178.42)	177.88	177.82	177.55	179.05	178.60	178.62	178.09	
	freq	A_1	1922.8 (1919.0)	1925.8	1938.7	1941.8	1880.5	1903.1	1897.5	1893.8	
		B_2	1842.9 (1838.6)	1846.6	1859.1	1860.6	1806.2	1829.1	1824.0	1820.3	
	μ		6.256 (6.321)	6.476	6.475	6.476	6.308	6.550	6.520	6.565	
	ΔE_{rel}[b]		27.8 (27.6)	32.0	27.8	37.7	6.8	10.6	7.5	8.9	
	ΔH_{rel}[c]		28.1 (27.9)	32.3	28.2	38.1	7.1	11.0	7.8	9.3	
$^3A_2$	geom[a]	r(Cr−C)	1.841 (1.841)	1.819	1.813	1.828	1.822	1.798	1.798	1.794	
		r(C−O)	1.159 (1.162)	1.160	1.159	1.157	1.175	1.175	1.176	1.176	
		∠CCrC	77.62 (77.70)	76.00	75.84	75.15	79.12	76.91	76.90	75.63	
		∠CrCO	176.60 (176.69)	176.21	176.12	176.12	177.11	176.78	176.79	176.35	
	freq	A_1	1930.0 (1923.8)	1934.3	1948.0	1943.5	1901.4	1923.0	1917.3	1913.6	
		B_2	1784.0 (1777.7)	1790.2	1807.0	1788.7	1784.9	1805.9	1802.6	1799.9	
	μ		6.148 (6.252)	6.397	6.373	6.500	5.832	6.112	6.053	6.114	
	$\langle S^2 \rangle$		2.346 (2.344)	2.335	2.283	2.479	2.094	2.093	2.081	2.092	
	ΔE_{rel}[d]		14.2 (14.3)	16.2	12.9	19.9	−3.6	−2.0	−4.8	−4.3	
	ΔH_{rel}[e]		14.3 (14.4)	16.3	13.1	20.0	−3.4	−1.7	−4.5	−4.0	
$^5A_1$	geom[a]	r(Cr−C)	1.980	1.961	1.950	1.973	1.947	1.925	1.922	1.921	
		r(C−O)	1.149	1.149	1.148	1.146	1.165	1.164	1.165	1.164	
		∠CCrC	113.46	110.74	109.86	110.91	112.26	108.75	108.99	108.37	
		∠CrCO	177.88	177.02	176.80	177.36	175.60	175.16	175.01	174.93	
	freq	A_1	1981.7	1986.8	1999.0	2001.1	1945.9	1966.6	1960.8	1957.0	1970.8,[h] 1982.1[i]
		B_2	1852.1	1861.5	1880.3	1851.4	1862.0	1884.8	1880.3	1877.0	1821.5,[h] 1832.9[i]
	μ		3.473	3.594	3.625	3.580	3.518	3.635	3.599	3.640	
	$\langle S^2 \rangle$		6.369	6.337	6.298	6.409	6.124	6.130	6.112	6.126	
	ΔE_{rel}[f]		3.2	5.3	3.8	7.2	−6.5	−4.1	−5.8	−5.2	
	ΔH_{rel}[g]		2.8	5.0	3.5	6.8	−6.7	−4.3	−5.9	−5.3	

[a] The molecular structures are depicted in Figure 5. [b] $\Delta E_{rel} = E(^1A_1) − E(^7\Pi_u)$. [c] $\Delta H_{rel} = H(^1A_1) − H(^7\Pi_u)$. [d] $\Delta E_{rel} = E(^3A_2) − E(^7\Pi_u)$. [e] $\Delta H_{rel} = H(^3A_2) − H(^7\Pi_u)$. [f] $\Delta E_{rel} = E(^5A_1) − E(^7\Pi_u)$. [g] $\Delta H_{rel} = H(^5A_1) − H(^7\Pi_u)$. [h] Reference 62, in solid argon. [i] Reference 62, in solid neon.
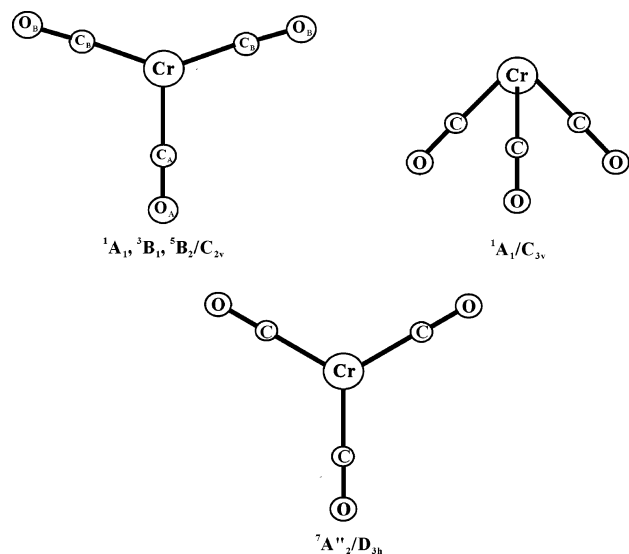
Figure 4. Molecular structures of Cr(CO)$_3$ (molecular state/molecular symmetry).

Figure 5. Molecular structures of Cr(CO)$_2$ (molecular state/molecular symmetry).

Figure 6. Molecular structures of CrCO (molecular state/molecular symmetry).

$^1A_{1g}$ for the mPW1PW91) However, in GGA functionals except BLYP, the order of the energy is $^1A_1 < ^3B_2 < ^3B_{1g} < ^1A_{1g} < ^5B_2$ ($^1A_1 < ^3B_2 < ^1A_{1g} < ^3B_{1g} < ^5B_2$ for BLYP). The main difference is the order of the $^1A_{1g}$ state and $^5B_2$ state. The hybrid functionals contain exact part of exchange energies calculated explicitly, which usually favor high spin state such as quintet. This is consistent with the results that with hybrid functionals, the $^5B_2$ state is more stable than the $^1A_{1g}$ state. All functionals give the same trend that square planar structures ($^1A_{1g}$ and $^3B_{1g}$) are somewhat unstable in comparison to the seesaw structure ($^1A_1$ and $^3B_2$).

4. Cr(CO)$_3$. Experiments suggested that Cr(CO)$_3$ in CH$_4$ matrix has C_{3v} symmetry.[98] Transient time-resolved infrared absorption in the gas phase showed that Cr(CO)$_3$ is C_{3v} symmetric in its singlet spin state according to its rate constant.[46,70,71] The previous DFT study (BP86/6-311+G(d)) proposed that the ground state is $^1A_1$ with C_{3v} symmetry, in agreement with previous two experiments.[62] Our calculation also supports that the C_{3v} structure is a singlet spin state ($^1A_1$). However, the results with all hybrid functionals except the B3P86 indicates that the global minimum of Cr(CO)$_3$ is the C_{2v} symmetry with quintet ($^5B_2$) rather than C_{3v} ($^1A_1$). In contrast, the results with all GGA functionals give that the $^5B_2$ (C_{2v}) state has 1 imaginary frequency (all C_{3v} structures have no imaginary frequency) and it is less stable than $^1A_1$ (C_{3v}) state (see

TABLE 11: Geometrical Parameters^a (Lengths in Å, Angles in Deg), Stretching Vibrational Frequencies^b of C−O (cm^{-1}), Dipole Moment (Debye), $\langle S^2 \rangle$, Number of Imaginary Frequencies, and Relative Energies (kcal/mol) among $D_{\infty h}$ ($^5\Pi_g$), C_{2v} ($^5A_1$), and $D_{\infty h}$ ($^7\Pi_u$) Structures of Cr(CO)$_2$ from Calculations Using the 6-311+G(d) Basis Set (in Parentheses, Results of Single Point Calculation Using the 6-311+G(3df) Basis Set at Optimized Geometries Using the 6-311+G(d))

6-311+G(d)	B3LYP	B3PW91	B3P86	mPW1PW91	BLYP	BPW91	BP86	PBE	MP2	CCSD	CCSD(T)
					$D_{\infty h}$ ($^5\Pi_g$)						
r(Cr−C)	1.990	1.978	1.971	1.982	1.983	1.966	1.965	1.964	1.988	2.013	1.994
r(C−O)	1.150	1.150	1.149	1.147	1.165	1.163	1.164	1.164	1.163	1.149	1.158
Σ_g	2086.0	2102.0	2106.7	2127.7	1984.8	2009.4	2005.3	2011.4	2024.3	2112.3	1812.3
Σ_u	1881.4	1874.5	1899.2	1797.3	1881.7	1902.0	1900.8	1905.7	2158.3	509.9	1616.3
$\langle S^2 \rangle$	6.192	6.203	6.183	6.245	6.090	6.098	6.088	6.097	6.693	6.706 (6.704)	6.696 (6.693)
imag freq	0	0	0	0	0	0	0	0	0	1	2
$\Delta E_{rel}{}^c$	−2.8	−0.0049	−1.5	2.5	−12.6	−9.4	−11.0	−10.0	17.5	12.8 (11.1)	7.3 (4.8)
$\Delta H_{rel}{}^d$	−2.7	0.040	−1.4	2.4	−12.4	−9.2	−10.8	−9.9	17.5	10.2	5.2
					C_{2v} ($^5A_1$)						
r(Cr−C)	1.980	1.962	1.951	1.974	1.947	1.926	1.923	1.922	2.035	2.038	1.994
r(C−O)	1.152	1.152	1.151	1.149	1.168	1.167	1.168	1.168	1.160	1.148	1.159
∠CCrC	112.34	109.94	109.17	110.09	111.39	108.08	108.31	107.69	123.34	112.37	109.53
∠CrCO	177.68	176.77	176.51	177.08	175.36	174.90	174.74	174.72	176.86	179.94	177.97
A_1	2055.1	2070.2	2073.9	2092.9	1946.2	1969.1	1963.1	1970.6	2495.9	2053.3	1991.3
B_2	1924.0	1941.6	1951.7	1940.8	1861.6	1886.5	1881.8	1889.3	1961.9	2213.1	1964.4
μ	3.579	3.687	3.715	3.671	3.626	3.727	3.691	3.723	1.819	2.715	3.975
$\langle S^2 \rangle$	6.365	6.335	6.298	6.406	6.123	6.128	6.111	6.125	6.863	6.838 (6.837)	6.798 (6.797)
$\Delta E_{rel}{}^e$	3.0	5.1	3.6	6.9	−6.5	−4.2	−5.9	−5.3	17.1	13.5 (12.4)	9.6 (7.6)
$\Delta H_{rel}{}^f$	2.7	4.8	3.3	6.6	−6.7	−4.4	−6.0	−5.5	17.0	13.4	9.3
					$D_{\infty h}$ ($^7\Pi_u$)						
r(Cr−C)	2.050	2.038	2.030	2.038	2.049	2.033	2.030	2.030	2.044	2.064	2.057
r(C−O)	1.150	1.149	1.148	1.145	1.166	1.163	1.164	1.164	1.154	1.143	1.152
Σ_g	2056.0	2076.3	2080.4	2098.6	1954.8	1984.0	1977.8	1986.3	2079.2	2093.3	2031.8
Σ_u	1982.1	2007.4	2010.8	2025.2	1896.2	1929.1	1923.0	1932.1	2101.9	1999.8	1961.9
$\langle S^2 \rangle$	12.006	12.008	12.008	12.009	12.004	12.007	12.006	12.006	12.032	12.029 (12.030)	12.030 (12.031)

^{a} The molecular structures are depicted in Figure 5. ^{b} Unscaled value. ^{c} $\Delta E_{rel} = E(^5\Pi_g) - E(^7\Pi_u)$. ^{d} $\Delta H_{rel} = H(^5\Pi_g) - H(^7\Pi_u)$. ^{e} $\Delta E_{rel} = E(^5A_1) - E(^7\Pi_u)$. ^{f} $\Delta H_{rel} = H(^5A_1) - H(^7\Pi_u)$.

Tables 6 and 7). As noted above for Cr(CO)$_4$, the exact exchange part calculated like HF exchange terms might make high spin state more stable. Under the frozen orbital approximation, the exchange interaction of the quintet is larger than that of the singlet, and the same may hold for a relaxed set of orbitals. All calculations using hybrid functionals give that all C_{2v} ($^5B_2$) structures are more stable than C_{3v} ($^1A_1$) structures. According to these results, introducing the exact exchange energy affects the potential energy surface of high spin states more than that of low spin states.

To clarify our DFT results, we performed calculations of the $^5B_2$ (C_{2v}) and $^1A_1$ (C_{3v}) states using ab initio methods. The results are summarized in Table 8. The C_{2v} ($^5B_2$) structure calculated using the MP2 method has 1 imaginary frequency and the C_{3v} ($^1A_1$) structure is more stable than the C_{2v} ($^5B_2$) structure (see Table 8). However, in the CCSD calculation, the relative stability is reversed and the C_{2v} ($^5B_2$) structure has no imaginary frequency. These results favor the C_{2v} ($^5B_2$) structure as the ground state.

However, we should consider spin contamination. As shown in Tables 6−8, spin contamination is not negligible in the triplet and quintet states. In general, the spin contamination of hybrid functionals is larger than that of GGA functionals because of the exact exchange energy in the former. Ab initio methods suffer more spin contamination than DFT ones in the $^5B_2$ (C_{2v}) state (see Table 8). Although the CCSD calculation show that the $^5B_2$ (C_{2v}) state is more stable than the $^1A_1$ (C_{3v}) state, the former might not be the ground state of Cr(CO)$_3$ because its wavefunction is contaminated by other spin states. Therefore, further work should be carried out to clarify the ground state of Cr(CO)$_3$ using multireference based method.

For the $^1A_1$ (C_{3v}) state, the B3LYP functional reproduces experimental results well, and GGAs except BLYP also give good results (see Table 7). The CCSD method provides an excellent result (1976.6 × 0.954 = 1885.7), which agrees well with the experiment value (see Tables 7 and 8). The MP2 method underestimates the frequency (1928.2 × 0.950 = 1831.8).

5. Cr(CO)$_2$. Cr(CO)$_2$ was fully optimized with DFT methods using the 6-311+G(3df) basis set and the results are summarized in Tables 9 and 10 and Figure 5. The previous DFT calculation using BP86/6-311+G(d) showed that the ground state of Cr-(CO)$_2$ is a quintet with a linear structure ($^5\Pi_g$).[62] In our calculation, all DFT functionals except B3PW91 and mPW1PW91 also provide that $^5\Pi_g$ is the ground state. However, we note that the triplet and quintet states of Cr(CO)$_2$ suffer considerable spin contamination, as shown in Tables 9 and 10. To clarify the true ground state, we carried out further ab initio calculations with 6-311+G(d) and additional DFT calculations with the same basis set for comparison. The results are summarized in Table 11. All ab initio methods yielded the contrary result that $^5\Pi_g$ is less stable than septet ($^7\Pi_u$) in the linear structure. Especially, the energy difference is 7.3 kcal/mol at the CCSD-(T)/6-311+G(d) level. Therefore, we conclude that the ground state of Cr(CO)$_2$ is $^7\Pi_u$, but further work using a multireference based method should be performed to resolve relative stability of all species.

In a previous experiment, Andrews et al. showed that vibrational frequencies of Cr(CO)$_2$ approximately match the calculated values for $^5A_1$.[62] As shown in Table 10, the B3LYP functional gives good results for the A_1 mode. Other hybrid functionals overestimate, whereas all GGA functionals underestimate, the frequency. However, for the B_2 mode, all functionals overestimate the frequency and both hybrid and GGA functionals give similar results. Actually, the possibility of incorrect assignment cannot be ruled out. Because previous experiments were conducted in a matrix environment, interaction with matrix might come into play. The influence of the noble gas on the geometry is negligible, but the interaction energy between the metal and the noble gas is about 8−9 kcal/mol.[99]

TABLE 12: Geometrical Parameters^a (Lengths in Å, Angles in Deg), Stretching Vibrational Frequencies^b of C−O (cm^{-1}), Dipole Moment (Debye), and Relative Energies (kcal/mol) of Asymmetric Structures (^{5}A) of Cr(CO)$_2$

^{5}A	r(Cr−C$_A$)	r(C$_A$−O$_A$)	r(Cr−C$_B$)	r(C$_B$−O$_B$)	∠C$_B$CrC$_A$	∠CrC$_A$O$_A$	∠CrC$_B$O$_B$	A (cm^{-1})	μ	$\langle S^2 \rangle$	$\Delta E_{rel}{}^c$	$\Delta H_{rel}{}^d$
CCSD	2.094	1.131	1.999	1.173	180.00	179.95	179.99	2185.8, 1918.4	5.402	6.944	−3.6	−1.3
CCSD(T)	2.050	1.142	1.990	1.174	179.53	179.99	179.96	2067.0, 1858.8	7.413	6.944	0.5	2.4

^{a} The molecular structures are depicted in Figure 5. ^{b} Unscaled value. ^{c} $\Delta E_{rel} = E(^5A) − E(^5\Pi_g)$. ^{d} $\Delta H_{rel} = H(^5A) − H(^5\Pi_g)$.

TABLE 13: Geometrical Parameters (Lengths in Å, Angles in Deg), Scaled C−O Stretching Vibrational Frequencies (cm^{-1}), Dipole Moment (Debye), $\langle S^2 \rangle$, Number of Imaginary Frequencies, and Relative Energies (kcal/mol) of Linear Structures ($^1\Sigma$, $^3\Sigma$, $^5\Pi$, and $^7\Sigma$) of CrCO from DFT Calculations Using the 6-311+G(3df) Basis Set (in Parentheses, Calculated Results Using the 6-311+G(d) Basis Set)

			hybrid				GGA			
			B3LYP	B3PW91	B3P86	mPW1PW91	BLYP	BPW91	BP86	PBE
$^1\Sigma$	geom^a	r(Cr−C)	1.785 (1.784)	1.732	1.728	1.733	1.781	1.728	1.729	1.724
		r(C−O)	1.172 (1.179)	1.154	1.153	1.150	1.188	1.172	1.173	1.173
	freq	Σ	1807.7 (1810.0)	1935.4	1947.5	1949.2	1792.2	1920.5	1916.1	1912.8
	μ		5.269 (6.259)	3.050	3.084	2.958	4.638	3.347	3.287	3.362
	imag freq		0 (0)	0	0	0	1	0	0	0
	$\Delta E_{rel}{}^b$		72.4 (72.9)	101.5	96.2	106.0	55.1	87.7	81.1	83.9
	$\Delta H_{rel}{}^c$		73.0 (73.6)	102.4	97.0	106.8	55.0	88.5	81.9	84.7
$^3\Sigma$	geom^a	r(Cr−C)	1.799 (1.769)	1.827	1.822	1.833	1.765	1.744	1.816	1.811
		r(C−O)	1.183 (1.171)	1.166	1.164	1.164	1.186	1.186	1.181	1.181
	freq	Σ	1777.0 (1839.0)	1846.1	1864.1	1851.7	1824.4	1845.8	1843.5	1836.2
	μ		6.954 (4.634)	4.749	4.694	4.921	4.673	4.862	4.429	4.514
	$\langle S^2 \rangle$		2.368 (2.110)	3.207	3.184	3.286	2.051	2.061	3.065	3.075
	$\Delta E_{rel}{}^d$		47.4 (43.9)	43.9	40.6	46.6	29.2	36.7	28.6	31.1
	$\Delta H_{rel}{}^e$		47.8 (44.6)	44.5	41.1	47.1	29.9	37.3	29.1	31.6
$^5\Pi$	geom^a	r(Cr−C)	1.899 (1.899)	1.889	1.879	1.901	1.864	1.848	1.844	1.844
		r(C−O)	1.168 (1.171)	1.168	1.167	1.167	1.179	1.179	1.179	1.179
	freq	Σ	1866.7 (1857.8)	1871.2	1886.1	1878.6	1853.3	1874.7	1871.1	1867.5
	μ		4.957 (5.103)	5.133	5.070	5.375	4.345	4.494	4.423	4.496
	$\langle S^2 \rangle$		6.477 (6.475)	6.506	6.469	6.586	6.187	6.214	6.184	6.208
	imag freq		1 (1)	0	0	0	0	0	0	0
	$\Delta E_{rel}{}^f$		12.5 (12.9)	14.7	13.1	15.5	5.6	8.5	6.6	7.6
	$\Delta H_{rel}{}^g$		12.3 (12.6)	15.2	13.5	16.0	6.1	9.0	7.1	8.1
$^7\Sigma$	geom^a	r(Cr−C)	2.192 (2.203)	2.172	2.157	2.178	2.163	2.140	2.131	2.128
		r(C−O)	1.132 (1.135)	1.131	1.131	1.128	1.149	1.148	1.149	1.148
	freq	Σ	2045.4 (2036.6)	2050.6	2061.6	2069.5	1996.0	2019.5	2012.3	2009.4
	μ		1.676 (1.645)	1.797	1.731	1.926	1.143	1.316	1.273	1.313
	$\langle S^2 \rangle$		12.001 (12.001)	12.002	12.002	12.002	12.001	12.002	12.002	12.001
	imag freq		2 (2)	2	2	2	2	2	2	2
	$\Delta E_{rel}{}^h$		2.5 (2.9)	2.2	2.3	2.1	2.9	2.6	2.5	2.6
	$\Delta H_{rel}{}^i$		1.7 (2.1)	1.4	1.5	1.3	2.0	1.7	1.7	1.8

^{a} The molecular structures are depicted in Figure 6. ^{b} $\Delta E_{rel} = E(^1\Sigma) − E(^7A')$. ^{c} $\Delta H_{rel} = H(^1\Sigma) − H(^7A')$. ^{d} $\Delta E_{rel} = E(^3\Sigma) − E(^7A')$. ^{e} $\Delta H_{rel} = H(^3\Sigma) − H(^7A')$. ^{f} $\Delta E_{rel} = E(^5\Pi) − E(^7A')$. ^{g} $\Delta H_{rel} = H(^5\Pi) − H(^7A')$. ^{h} $\Delta E_{rel} = E(^7\Sigma) − E(^7A')$. ^{i} $\Delta H_{rel} = H(^7\Sigma) − H(^7A')$.

There is a possibility that these interactions may perturb the relative stability.[62]

Cr(CO)$_2$ can adopt a nonet state ($^9\Sigma_u$) in the linear structure. As shown in Table 9, the C−O bond length is somewhat longer, and the Cr−C bond length is shorter than those of other states, which implies a partial breakage of C−O bonds. This partial breaking can be rationalized by considering that the nonet state is formed from the septet state by moving one electron in the HOMO of the β spin orbital into the LUMO of α spin orbital of the septet state. Because the LUMO of α spin orbital has strong bonding character between Cr and C and antibonding character between C and O, and the HOMO of β spin orbital has bonding character for both pairs (see Figure 3S in Supporting Information), the $^9\Sigma_u$ state gains antibonding character between C and O and bonding character between Cr and C compared to the septet state. As a consequence, the C−O bond length is elongated and the Cr−C bond length is shortened. A similar trend occurs also in the nonet state of CrCO.

6. CrCO. Experimentally, CrCO was detected in an Ar matrix at 4 K and the observed stretching frequency was 1977 cm^{-1}.[100] Like other species, there is no other experimental structural information. There is experimental evidence that the ground state of CrCO is a septet and its dissociation energy is less than

1.5 kcal/mol.[50] Previous DFT studies suggested that the bent structure with a septet is the global minimum of CrCO species.[55,60,61] However, previous ab initio calculations showed that the global minimum is a linear structure and a septet.[58,59] Recently, CrCO was calculated using CCSD(T) with a large basis set. This result indicated that CrCO is bent and a septet.[101] However, this investigation did not contain any information about frequency. In the case of the ground state of CrCO, we clearly resolved these discrepancies in our recent work and showed that the ground state is septet in a bent structure ($^7A'$).[72]

In this work, we investigated all possible spin states and the corresponding structures are summarized in Tables 13 and 14. The results with all functionals show that a bent structure with a septet is the global minimum ($^7A'$). Its linear structure with septet ($^7\Sigma$) has two imaginary frequencies and is less stable than the bent structure ($^7A'$). These results are similar to those of previous DFT calculations.[55,60,61] As shown in Tables 13 and 14, open shell species except the septet and nonet have considerable spin contamination, and further study using multireference based method is required for triplet and quintet states.

The nonet state ($^9A''$) structure has substantially longer Cr−C and C−O bond lengths than other states as shown in Table 14.

TABLE 14: Geometrical Parameters (Lengths in Å, Angles in Deg), Scaled C–O Stretching Vibrational Frequencies (cm^{-1}), Dipole Moment (Debye), ⟨S^2⟩, and Relative Energies (kcal/mol) of Bent Structures (^{1}A′, ^{3}A″, ^{5}A′, ^{7}A′, and ^{9}A″) of CrCO from DFT Calculations Using 6-311+G(3df) Basis Set (in Parentheses, Calculated Results Using the 6-311+G(d) Basis Set)

			hybrid			GGA				
			B3LYP	B3PW91	B3P86	mPW1PW91	BLYP	BPW91	BP86	PBE	exp
^{1}A′	geom^a	r(Cr–C)	1.791 (1.789)	1.731	1.728	1.732	1.748	1.727	1.729	1.723	
		r(C–O)	1.172 (1.177)	1.154	1.153	1.150	1.172	1.172	1.173	1.173	
		∠CrCO	177.32 (177.50)	178.03	178.29	178.06	178.42	178.27	178.94	178.01	
	freq	A′	1771.8 (1766.7)	1936.3	1948.5	1950.4	1902.6	1922.5	1916.2	1914.1	
	μ		5.632 (5.804)	3.051	3.084	2.959	3.107	3.348	3.286	3.361	
	$\Delta E_{rel}{}^b$		72.7 (72.8)	101.6	96.2	106.0	75.2	87.7	81.1	84.0	
	$\Delta H_{rel}{}^c$		72.7 (72.8)	101.9	96.6	106.4	75.5	88.1	81.5	84.3	
^{3}A″	geom^a	r(Cr–C)	1.799 (1.769)	1.751	1.748	1.753	1.807	1.785	1.788	1.810	
		r(C–O)	1.183 (1.171)	1.169	1.168	1.166	1.180	1.180	1.181	1.181	
		∠CrCO	178.54 (177.53)	177.57	177.89	177.58	177.71	177.25	177.85	177.69	
	freq	A′	1776.6 (1839.6)	1850.2	1865.0	1855.0	1812.0	1844.6	1843.3	1837.5	
	μ		6.954 (4.633)	4.790	4.787	4.814	4.168	4.463	4.434	4.512	
	⟨S^2⟩		2.367 (2.110)	2.131	2.111	2.168	2.799	2.827	2.840	3.074	
	$\Delta E_{rel}{}^d$		47.4 (43.9)	50.0	46.1	53.7	23.2	30.0	25.7	31.1	
	$\Delta H_{rel}{}^e$		47.4 (44.2)	50.2	46.3	53.9	23.3	30.2	25.9	31.2	
^{5}A′	geom^a	r(Cr–C)	2.043 (2.042)	1.996	1.979	2.024					
		r(C–O)	1.139 (1.145)	1.147	1.147	1.139					
		∠CrCO	165.95 (164.02)	165.21	166.04	164.60					
	freq	A′	1866.9 (1838.4)	1633.8	1605.9	1664.9					
	μ		0.661 (0.805)	1.465	1.691	0.916					
	⟨S^2⟩		6.736 (6.735)	6.712	6.675	6.777					
	$\Delta E_{rel}{}^f$		9.8 (10.1)	16.0	13.9	16.5					
	$\Delta H_{rel}{}^g$		9.7 (10.1)	15.6	13.5	16.1					
^{7}A′	geom^a	r(Cr–C)	2.205 (2.213)	2.189	2.171	2.197	2.166	2.148	2.136	2.134	
		r(C–O)	1.142 (1.146)	1.141	1.141	1.137	1.159	1.157	1.158	1.158	
		∠CrCO	139.48 (137.47)	140.48	140.54	140.32	140.33	141.52	141.70	141.51	
	freq	A′	1946.8 (1935.0)	1956.6	1965.5	1970.2	1910.4	1937.1	1929.7	1925.7	1977;^{j} 1975.3^k
	μ		0.767 (0.827)	0.745	0.768	0.762	0.905	0.797	0.801	0.825	
	⟨S^2⟩		12.004 (12.004)	12.005	12.004	12.005	12.003	12.003	12.003	12.003	
^{9}A″	geom^a	r(Cr–C)	2.258 (2.256)	2.263	2.245	2.251	2.283	2.286	2.265	2.266	
		r(C–O)	1.273 (1.280)	1.259	1.261	1.260	1.282	1.265	1.270	1.267	
		∠CrCO	95.73 (97.09)	92.19	91.01	87.95	100.79	99.91	99.58	98.61	
	freq.	A′	1210.9 (1175.7)	1309.7	1312.4	1308.3	1255.7	1357.3	1332.4	1352.9	
	μ		2.553 (2.744)	2.369	2.307	2.327	2.195	2.127	2.042	2.081	
	⟨S^2⟩		20.009 (20.009)	20.008	20.007	20.008	20.006	20.005	20.005	20.005	
	$\Delta E_{rel}{}^h$		136.2 (135.3)	133.0	134.8	132.3	135.6	132.3	134.4	133.1	
	$\Delta H_{rel}{}^i$		135.1 (134.2)	132.1	133.8	131.3	134.6	131.4	133.5	132.2	

^{a} The molecular structures are depicted in Figure 6. ^{b} $\Delta E_{rel} = E(^1A') - E(^7A')$. ^{c} $\Delta H_{rel} = H(^1A') - H(^7A')$. ^{d} $\Delta E_{rel} = E(^3A'') - E(^7A')$. ^{e} $\Delta H_{rel} = H(^3A'') - H(^7A')$. ^{f} $\Delta E_{rel} = E(^5A') - E(^7A')$. ^{g} $\Delta H_{rel} = H(^5A') - H(^7A')$. ^{h} $\Delta E_{rel} = E(^9A'') - E(^7A')$. ^{i} $\Delta H_{rel} = H(^9A'') - H(^7A')$. ^{j} Reference 100. IR spectroscopy in Ar matrices at 4 K. ^{k} Reference 106. Laser-ablated generated Cr atoms reacting with CO$_2$ and isolated in Ar matrices.

This partial bond breaking of C–O can be rationalized in the same manner as in the nonet state of Cr(CO)$_2$. The LUMO of the α spin orbital in the septet state has antibonding character for Cr–C and C–O whereas the HOMO of β spin orbital has bonding character (see Figure 4S in Supporting Information). Because the ^{9}A″ state can be considered to be formed from the septet state by moving one electron from the HOMO of β spin orbital to the LUMO of α spin orbital of the septet as in Cr-(CO)$_2$, the bonding character for Cr–C and C–O is weakened and the corresponding bond lengths are elongated.

As shown in Tables 13 and 14, all linear structures in the quintet and septet states are less stable than the bent structure in each spin state. The results of NBO analysis are listed in Table 6S in the Supporting Information. The stability of the bent structure can be correlated with its stronger s character in Cr–C bonding compared with that in the linear structure.

B. Bond Dissociation Energy and Total CO Binding Energy. The sequential bond dissociation energies (BDEs) of Cr(CO)$_n$ (n = 1–6) are summarized in Table 15. In this work, we used ΔH at 298 K because this quantity is commonly designated as the BDE.[102,103] All calculations provide reasonable BDEs of Cr(CO)$_6$ that agree well with the experimental value but overestimate the BDE of Cr(CO)$_5$. An exception is found in the B3LYP and BLYP functionals, which give relatively good

results. There is uncertainty in determining the BDE of Cr(CO)$_4$ due to the fact that the ground state of Cr(CO)$_3$ is not known, but the BDEs calculated using hybrid functionals for both possibilities (Cr(CO)$_4$(^{1}A$_1$) → Cr(CO)$_3$(^{5}B$_2$) + CO and Cr(CO)$_4$-(^{1}A$_1$) → Cr(CO)$_3$(^{1}A$_1$) + CO) are close to the experimental value. The performance of GGA is worse in this regard. Even more possibilities arise for the BDE of Cr(CO)$_3$. All calculations using GGA functionals overestimate the experimental BDE for all channels, and those using hybrid functionals provide values slightly closer to the experimental one. The calculated BDEs of Cr(CO)$_2$ are underestimated compared with the experiment. Recently, we satisfactorily reproduced the BDE of CrCO using CCSD(T) in our previous study.[72] When the products (Cr(CO)$_6$ and Cr(CO)$_5$) are all singlets, the BDEs calculated by DFT methods are reasonable. However, if the products contain open shell character, the calculations using hybrid functionals generally underestimate the BDEs because of the preference for high spin states. In contrast, generally the results with GGA functionals overestimate the BDEs.

The total CO binding energies for Cr(CO)$_6$ are summarized in Table 15. The experimental value corresponding to D_o^{298} is 153 kcal/mol.[104] Whereas the results with GGA functionals seriously overestimate the experimental value, the B3PW91 and

TABLE 15: Sequential Bond Dissociation Energy (ΔH)^a of $Cr(CO)_n$ ($n = 1$–6) Species and Total Binding Energy (ΔH)^a (kcal/mol) from DFT Calculations Using the 6-311+G(3df) Basis Set (in Parentheses, Calculated Results Using the 6-311+G(d) Basis Set)

	hybrid				GGA				exp
	B3LYP	B3PW91	B3P86	mPW1PW91	BLYP	BPW91	BP86	PBE	
$Cr(CO)_6\,(^1A_{1g}) \rightarrow Cr(CO)_5\,(^1A_1) + CO(^1\Sigma^+)$	34.6/33.9 (34.4/33.3)	38.6/37.7	40.6/39.7	39.6/38.7	34.8/34.0	39.5/38.6	40.9/40.1	42.8/42.0	37($\pm$2),^{b} 37($\pm$5)^c
$Cr(CO)_5\,(^1A_1) \rightarrow Cr(CO)_4\,(^1A_1) + CO(^1\Sigma^+)$	34.2/33.5 (33.9/32.8)	37.0/36.1	38.9/38.0	37.8/36.9	34.9/34.2	38.3/37.4	39.8/39.0	41.3/40.5	25 $\pm$ 5,^{c} 33^f
$Cr(CO)_4\,(^1A_1) \rightarrow Cr(CO)_3\,(^5B_2) + CO(^1\Sigma^+)$	30.3/29.6 (29.7/28.8)	33.7/32.9	37.9/37.1	30.5/29.6	44.9/44.2	50.4/49.5	52.7/51.9	54.7/53.9	
$Cr(CO)_4\,(^1A_1) \rightarrow Cr(CO)_3\,(^1A_1) + CO(^1\Sigma^+)$	35.0/34.3 (34.5/33.6)	37.2/36.4	38.9/38.1	37.8/36.9	36.3/35.7	39.1/38.2	40.4/39.6	41.8/41.0	32.1^d
$Cr(CO)_3\,(^5B_2) \rightarrow Cr(CO)_2\,(^5A_1) + CO(^1\Sigma^+)$	29.6/29.1 (28.9/28.4)	31.0/30.3	33.2/32.5	30.5/29.8	33.5/32.9	35.3/34.6	37.1/36.4	37.9/37.3	
$Cr(CO)_3\,(^1A_1) \rightarrow Cr(CO)_2\,(^5A_1) + CO(^1\Sigma^+)$	24.9/24.3 (24.2/23.4)	27.5/26.7	32.1/31.4	23.2/22.4	42.0/41.4	46.6/45.8	49.4/48.6	50.8/50.0	
$Cr(CO)_3\,(^5B_2) \rightarrow Cr(CO)_2\,(^7\Pi_g) + CO(^1\Sigma^+)$	26.8/26.2 (26.2/25.7)	26.0/25.8	29.6/29.5	23.7/22.9	40.1/39.6	39.6/38.9	43.0/42.3	43.2/42.6	28.4^d
$Cr(CO)_3\,(^1A_1) \rightarrow Cr(CO)_2\,(^7\Pi_g) + CO(^1\Sigma^+)$	22.0/21.4 (21.5/20.7)	22.5/21.7	28.6/27.8	16.4/15.6	48.7/48.0	50.9/50.1	55.3/54.5	56.1/55.3	
$Cr(CO)_2\,(^5A_1) \rightarrow CrCO\,(^7A') + CO(^1\Sigma^+)$	13.6/13.0 (12.8/12.3)	12.3/11.6	16.2/15.6	10.6/10.0	25.6/25.1	24.4/23.8	28.4/27.6	28.4/27.8	28.4^d
$Cr(CO)_2\,(^7\Pi_g) \rightarrow CrCO\,(^7A') + CO(^1\Sigma^+)$	16.4/15.9 (15.5/14.9)	17.3/16.6	19.7/19.1	17.5/16.8	19.0/18.4	20.2/19.5	22.3/21.7	23.1/22.4	
$CrCO\,(^7A') \rightarrow Cr(^7S) + CO(^1\Sigma^+)$	6.5/6.2 (6.1/5.9)	6.2/5.8	8.4/7.9	5.9/5.5	11.3/10.9	10.9/10.5	13.3/12.8	13.6/13.2	1.5 <^{e}
$Cr(CO)_6\,(^1A_{1g}) \rightarrow Cr(^7\Sigma) + 6CO(^1\Sigma^+)$	148.9/146.7 (145.9/143.9)	158.8/156.4	175.1/172.7	155.0/152.5	184.9/182.7	198.9/196.3	212.0/209.6	218.7/216.3	153^g

^{a} Normal value/BSSE corrected value. ^{b} Reference 44. ^{c} Reference 47. ^{d} Reference 44. ^{e} Reference 53. ^{f} Reference 50. ^{g} Reference 107. Reference 104.

mPW1PW91 functionals provide reasonable values. In general, hybrid functionals give more accurate results.

Conclusions

For a comparison with experimental intermediate structures provided by time-resolved diffraction experiment, we carried out geometry optimizations of $Cr(CO)_n$ species ($n = 1$–6) for all possible spin states and calculated sequential bond dissociation energies, total CO binding energies and C−O stretching frequencies using various density functional methods with the 6-311+G(3df) basis set. All functionals provide results that show good agreement with the available experimental data for $Cr(CO)_n$ ($n = 4$–6). In addition, the ground states of $Cr(CO)_5$ and $Cr(CO)_4$ agree well with the experimental results. To clarify important issues for other $Cr(CO)_n$ species ($n = 2$–3), we used high-level ab initio methods and various DFT functionals. For $Cr(CO)_3$, we propose a new lowest-energy state that is not a C_{3v} structure in the singlet state but rather a C_{2v} structure in the quintet state. For the $Cr(CO)_2$ case, the lowest-energy state is a linear septet rather than a quintet. In the quintet state, $Cr(CO)_2$ also has an asymmetric structure. In this work, our investigation shows that the DFT methods can provide accurate geometries and bond energies for transition metal system whose ground state is singlet with cost-effectiveness. In the case of the high spin state whose multiconfigurational character becomes significant, however, DFT methods do not find the lowest-energy state quite as well. We hope this work could aid further experimental studies of $Cr(CO)_n$ ($n = 2$–5), which have not yet been undertaken.

Supporting Information Available: The results of diatomic CO using various ab initio methods and DFT functional and discussions are in Table 1S. The NPA charges of all species are summarized in Table 2S, 3S, 5S, 7S, 9S, and 11s. The results of NBO analysis about all species at the B3LYP/6-311+G(d) level (Tables 4S, 6S, 8S, 10S, and 12S). Additional structures of $Cr(CO)_3$ and $Cr(CO)_4$ are shown in Figures 1S and 2S. In Table 13S, we summarize the results of the atomic state of Cr using various DFT functionals. The HOMO of the α spin orbital and the LUMO of the β spin orbital of the nonet state of $Cr(CO)_2$ ($^9\Sigma_u$) and $CrCO$ ($^9A''$) are depicted in Figures 3S and 4S. This material is available free of charge via the Internet at http://pubs.acs.org.

References and Notes

(1) Hoffmann, R. *Angew. Chem., Intl. Ed. Engl.* **1982**, *21*, 711.

(2) Wilkinson, G. *Comprehensive Organometallic Chemistry,*; Pergamon: Oxford, 1982; Vols. 1−9.

(3) Ihee, H.; Lobastov, V. A.; Gomez, U. M.; Goodson, B. M.; Srinivasan, R.; Ruan, C.; Zewail, A. H. *Science* **2001**, *291*, 458.

(4) Dudek, R. C.; Weber, P. M. *J. Phys. Chem. A* **2001**, *105*, 4167.

(5) Siwick, B. J.; Dwyer, J. R.; Jordan, R. E.; Miller, R. J. D. *Science* **2003**, *302*, 1382.

(6) Ruan, C.; Lobastov, V. A.; Vigliotti, F.; Chen, S.; Zewail, A. H. *Science* **2004**, *304*, 80.

(7) Boronat, M.; Viruela, P.; Corma, A. *J. Phys. Chem. A* **1998**, *102*, 982.

(8) Niu, S.; Thomson, L. M.; Hall, M. B. *J. Am. Chem. Soc.* **1999**, *121*, 4000.

(9) Fraile, J. M.; Garcia, J. I.; Martinez-Merino, V.; Mayoral, J. A.; Salvatella, L. *J. Am. Chem. Soc.* **2001**, *123*, 7616.

(10) Ihee, H.; Cao, J.; Zewail, A. H. *Chem. Phys. Lett.* **1997**, *281*, 10.

(11) Ihee, H.; Cao, J.; Zewail, A. H. *Angew. Chem., Intl. Ed. Engl.* **2001**, *40*, 1532.

(12) Ihee, H.; Feenstra, J. S.; Cao, J.; Zewail, A. H. *Chem. Phys. Lett.* **2002**, *353*, 325.

(13) Ihee, H.; Goodson, B. M.; Srinivasan, R.; Lobastov, V. A.; Zewail, A. H. *J. Phys. Chem. A* **2002**, *106*, 4087.

(14) Ihee, H.; Lorenc, M.; Kim, T. K.; Kong, Q. Y.; Cammarata, M.; Lee, J. H.; Bratos, S.; Wulff, M. *Science* **2005**, *309*, 1223.

(15) Kim, T. K.; Lorenc, M.; Lee, J. H.; Lo, Russo, M.; Kim, J.; Cammarata, M.; Kong, Q.; Noel, S.; Plech, A.; Wulff, M.; Ihee, H. *Proc. Natl. Acad. Sci. U.S.A.* **2006**, *103*, 9410.

(16) Park, S. T.; Feenstra, J. S.; Zewail, A. H. *J. Chem. Phys.* **2006**, *124*, 174707.

(17) Ziegler, T.; Tschinke, V.; Ursenbach, C. *J. Am. Chem. Soc.* **1987**, *109*, 4825.

(18) Barnes, L. A.; Rosi, M.; Bauschlicher, C. W., Jr. *J. Chem. Phys.* **1991**, *94*, 2031.

(19) Fan, L.; Ziegler, T. *J. Chem. Phys.* **1991**, *95*, 7401.

(20) Sosa, C.; Andzelm, J.; Elkin, B. C.; Wimmer, E.; Dobbs, K. D.; Dixon, D. A. *J. Phys. Chem.* **1992**, *96*, 6630.

(21) Lin, Z.; Hall, M. B. *Inorg. Chem.* **1992**, *31*, 2791.

(22) Fan, L.; Ziegler, T. *J. Phys. Chem.* **1992**, *96*, 6937.

(23) Barnes, L. A.; Liu, B.; Lindh, R. *J. Chem. Phys.* **1993**, *98*, 3978.

(24) Davidson, E. R.; Kunze, K. L.; Machado, F. B. C.; Chakravorty, S. J. *Acc. Chem. Res.* **1993**, *26*, 628.

(25) Machado, F. B. C.; Davidson, E. R. *J. Phys. Chem.* **1993**, *97*, 4397.

(26) Persson, B. J.; Roos, B. O.; Pierloot, K. *J. Chem. Phys.* **1994**, *101*, 6810.

(27) Li, J.; Schreckenbach, G.; Ziegler, T. *J. Phys. Chem.* **1994**, *98*, 4838.

(28) Ehlers, A. W.; Frenking, G. *J. Am. Chem. Soc.* **1994**, *116*, 1514.

(29) Delley, B.; Wrinn, M.; Luthi, H. P. *J. Chem. Phys.* **1994**, *100*, 5785.

(30) Berces, A.; Ziegler, T. *J. Phys. Chem.* **1994**, *98*, 13233.

(31) Dapprich, S.; Pidun, U.; Ehlers, A. W.; Frenking, G. *Chem. Phys. Lett.* **1995**, *242*, 521.

(32) Jonas, V.; Thiel, W. *J. Chem. Phys.* **1995**, *102*, 8474.

(33) Li, J.; Schreckenbach, G.; Ziegler, T. *J. Am. Chem. Soc.* **1995**, *117*, 486.

(34) van Wullen, C. *J. Chem. Phys.* **1996**, *105*, 5485.

(35) Rosa, A.; Ehlers, A. W.; Baerends, E. J.; Snijders, J. G.; Velde, G. t. *J. Phys. Chem.* **1996**, *100*, 5690.

(36) Ehlers, A. W.; Ruiz-Morales, Y.; Baerends, E. J.; Ziegler, T. *Inorg. Chem.* **1997**, *36*, 5031.

(37) Rolke, J.; Zheng, Y.; Brion, C. E.; Chakravorty, S. J.; Davidson, E. R.; McCarthy, I. E. *Chem. Phys.* **1997**, *215*, 191.

(38) Spears, K. G. *J. Phys. Chem. A* **1997**, *101*, 6273.

(39) Rosa, A.; Baerends, E. J.; van Gisbergen, S. J. A.; van Lenthe, E.; Groeneveld, J. A.; Snijders, J. G. *J. Am. Chem. Soc.* **1999**, *121*, 10356.

(40) Whitaker, A.; Jeffery, J. W. *Acta Crystallogr.* **1967**, *23*, 977.

(41) Jost, A.; Rees, B.; Yelon, W. B. *Acta Crystallogr.* **1975**, *B31*, 2649.

(42) Perutz, R. N.; Turner, J. J. *J. Am. Chem. Soc.* **1975**, *97*, 4791.

(43) Rees, B.; Mitschler, A. *J. Am. Chem. Soc.* **1976**, *98*, 7918.

(44) Lewis, K. E.; Golden, D. M.; Smith, G. P. *J. Am. Chem. Soc.* **1984**, *106*, 3905.

(45) Church, S. P.; Grevels, F.; Hermann, H.; Schaffner, K. *Inorg. Chem.* **1985**, *24*, 418.

(46) Seder, T. A.; Church, S. P.; Weitz, E. *J. Am. Chem. Soc.* **1986**, *108*, 4721.

(47) Fletcher, T. R.; Rosenfeld, R. N. *J. Am. Chem. Soc.* **1988**, *110*, 2097.

(48) Venkataraman, B.; Hou, H.; Zhang, Z.; Chen, S.; Bandukwalla, G.; Vernon, M. *J. Chem. Phys.* **1990**, *92*, 5338.

(49) Hansford, G. M.; Davies, P. B. *J. Chem. Phys.* **1996**, *104*, 8292.

(50) Trushin, S. A.; Sugawara, K.; Takeo, H. *Chem. Phys. Lett.* **1997**, *267*, 573.

(51) Willey, K. F.; Brummel, C. L.; Winograd, N. *Chem. Phys. Lett.* **1997**, *267*, 359.

(52) Gutmann, M.; Janello, J. M.; Dickebohm, M. S.; Grossekathofer, M.; Lindener-Roenneke, J. *J. Phys. Chem. A* **1998**, *102*, 4138.

(53) Trushin, S. A.; Fuss, W.; Schmid, W. E.; Kompa, K. L. *J. Phys. Chem. A* **1998**, *102*, 4129.

(54) Gutmann, M.; Dickebohm, M. S.; Janello, J. M. *J. Phys. Chem. A* **1999**, *103*, 2580.

(55) Adamo, C.; Lelj, F. *J. Chem. Phys.* **1995**, *103*, 10605.

(56) Adamo, C.; Lelj, F. *Chem. Phys. Lett.* **1995**, *246*, 463.

(57) Hay, P. J. *J. Am. Chem. Soc.* **1978**, *100*, 2411.

(58) Jeung, G.-H. *J. Am. Chem. Soc.* **1992**, *114*, 3211.

(59) Jeung, G.-H.; Haettel, S. *Int. J. Quantum. Chem.* **1997**, *61*, 547.

(60) Fournier, R. *J. Chem. Phys.* **1993**, *98*, 8041.

(61) Fournier, R. *J. Chem. Phys.* **1993**, *99*, 1801.

(62) Andrews, L.; Zhou, M.; Gutsev, G. L.; Wang, X. *J. Phys. Chem. A* **2003**, *107*, 561.

(63) Li, S.; King, R. B.; Schaefer, H. F., III. *J. Phys. Chem. A* **2004**, *108*, 6879.

(64) Li, S.; Richardson, N. A.; King, R. B.; Schaefer, H. F., III. *J. Phys. Chem. A* **2003**, *107*, 10118.

(65) Hyla-Kryspin, I.; Grimme, S. *Organometalics* **2004**, *23*, 5581.

(66) Fournier, R.; Papai, I. *Recent Advanced in Density Functional Methods Part I*; World Scientific: Singapore, 1995.

(67) Bauschlicher, C. W., Jr.; Ricca, A.; Partridge, H.; Langhoff, S. R. *Recent Advances in Density Functional methods Part II*; World Scientific: Singapore, 1997.

(68) Holthausen, M. C.; Mohr, M.; Koch, W. *Chem. Phys. Lett.* **1995**, *240*, 245.

(69) Rodriguez-Santiago, L.; Sodupe, M.; Branchadell, V. *J. Chem. Phys.* **1996**, *105*, 9966.

(70) Ishikawa, Y.; Brown, C. E.; Hackett, P. A.; Rayner, D. M. *J. Phys. Chem.* **1990**, *94*, 2404.

(71) Weitz, E. *J. Phys. Chem.* **1987**, *91*, 3945.

(72) Kim, J.; Lee, Y. S.; Ihee, H. *Int. J. Quantum. Chem.* **2007**, *107*, 458.

(73) Frisch, M. J.; Trucks, G. W.; Schlegel, H. B.; Scuseria, G. E.; Robb, M. A.; Cheeseman, J. R.; Montgomery, J. A., Jr.; Vreven, T.; Kudin, K. N.; Burant, J. C.; Millam, J. M.; Iyengar, S. S.; Tomasi, J.; Barone, V.; Mennucci, B.; Cossi, M.; Scalmani, G.; Rega, N.; Petersson, G. A.; Nakatsuji, H.; Hada, M.; Ehara, M.; Toyota, K.; Fukuda, R.; Hasegawa, J.; Ishida, M.; Nakajima, T.; Honda, Y.; Kitao, O.; Nakai, H.; Klene, M.; Li, X.; Knox, J. E.; Hratchian, H. P.; Cross, J. B.; Adamo, C.; Jaramillo, J.; Gomperts, R.; Stratmann, R. E.; Yazyev, O.; Austin, A. J.; Cammi, R.; Pomelli, C.; Ochterski, J. W.; Ayala, P. Y.; Morokuma, K.; Voth, G. A.; Salvador, P.; Dannenberg, J. J.; Zakrzewski, V. G.; Dapprich, S.; Daniels, A. D.; Strain, M. C.; Farkas, O.; Malick, D. K.; Rabuck, A. D.; Raghavachari, K.; Foresman, J. B.; Ortiz, J. V.; Cui, Q.; Baboul, A. G.; Clifford, S.; Cioslowski, J.; Stefanov, B. B.; Liu, G.; Liashenko, A.; Piskorz, P.; Komaromi, I.; Martin, R. L.; Fox, D. J.; Keith, T.; Al-Laham, M. A.; Peng, C. Y.; Nanayakkara, A.; Challacombe, M.; Gill, P. M. W.; Johnson, B.; Chen, W.; Wong, M. W.; Gonzalez, C.; Pople, J. A. *Gaussian 03*, revision A.1; Gaussian, Inc., Pittsburgh PA, 2003.

(74) Becke, A. D. *J. Chem. Phys.* **1993**, *98*, 5648.

(75) Lee, C.; Yang, W.; Parr, R. G. *Phys. Rev. B* **1988**, *37*, 785.

(76) Perdew, J. P. *Phys. Rev. B* **1986**, *33*, 8822.

(77) Adamo, C.; Barone, V. *J. Chem. Phys.* **1998**, *108*, 664.

(78) Perdew, J. P. *Electronic Structure of Solids*; Akademic Verlag: Berlin, 1991.

(79) Becke, A. D. *Phys. Rev. A* **1988**, *38*, 3098.

(80) Perdew, J. P.; Burke, K.; Enzerhof, M. *Phys. Rev. Lett.* **1996**, *77*, 3865.

(81) Wachters, A. J. H. *J. Chem. Phys.* **1970**, *52*, 1033.

(82) Hay, P. J. *J. Chem. Phys.* **1977**, *66*, 4377.

(83) Raghavachari, K.; Trucks, G. W. *J. Chem. Phys.* **1989**, *91*, 1062.

(84) Boys, S. F.; Bernardi, F. *Mol. Phys.* **1970**, *19*, 553.

(85) Frisch, M. J.; Head-Gordon, M.; Pople, J. A. *Chem. Phys. Lett.* **1990**, *166*, 281.

(86) Head-Gordon, M.; Head-Gordon, T. *Chem. Phys. Lett.* **1994**, *220*, 122.

(87) Purvis, G. D.; Bartlett, R. J. *J. Chem. Phys.* **1982**, *76*, 1910.

(88) Scuseria, G. E.; Janssen, C. L.; Schaefer, H. F., III. *J. Chem. Phys.* **1988**, *89*, 1988.

(89) Raghavachari, K.; Trucks, G. W.; Pople, J. A.; Head-Gordon, M. *Chem. Phys. Lett.* **1989**, *157*, 479.

(90) http://srdata.nist.gov/cccbdb/.

(91) Reed., A. E.; Curtis, L. A.; Weinhold., F. *Chem. Rev.* **1988**, *88*, 899.

(92) Perutz, R. N.; Turner, J. J. *Inorg. Chem.* **1975**, *14*, 262.

(93) Kundig, E. P.; Ozin, G. A. *J. Am. Chem. Soc.* **1974**, *96*, 3820.

(94) Demuynck, J.; Kochanski, E.; Veillard, A. *J. Am. Chem. Soc.* **1979**, *101*, 3467.

(95) Huheey, J. E.; Keiter, E. A.; Keiter, R. L. *Inorganic Chemistry*: *Principles of Structure and Reactivity*, 4th ed.; Harper Collins College Publishers: New York, 1993.

(96) Burdett, J. K.; Graham, M. A.; Perutz, R. N.; Poliakoff, M.; Rest, A. J.; Turner, J. J.; Turner, R. F. *J. Am. Chem. Soc.* **1975**, *97*, 4805.

(97) Fletcher, T. R.; Rosenfeld, R. N. *J. Am. Chem. Soc.* **1985**, *107*, 2203.

(98) Perutz, R. N.; Turner, J. J. *J. Am. Chem. Soc.* **1975**, *97*, 4800.

(99) Ehlers, A. W.; Frenking, G.; Baerends, E. J. *Organometallics* **1997**, *16*, 4896.

(100) Bach, S. B. H.; Taylor, C. A.; Zee, R. J. V.; Vala, M. T.; Weltner, H. J. *J. Am. Chem. Soc.* **1986**, *108*, 7104.

(101) Koukounas, C.; Kardahakis, S.; Mavridis, A. *J. Chem. Phys.* **2005**, *123*, 074327.

(102) Benson, S. W. *J. Chem. Educ.* **1965**, *42*, 502.

(103) McMillen, D. F.; Golden, D. M. *Ann. Rev. Phys. Chem.* **1982**, *33*, 493.

(104) Pittam, D. A.; Pilcher, G.; Barnes, D. S.; Skinner, H. A.; Todd, D. *J. Less-Common Met.* **1975**, *42*, 217.

(105) Jones, L. H.; McDowell, R. S.; Goldblatt, M. *Inorg. Chem.* **1969**, *8*, 2349.

(106) Souter, P. F.; Andrews, L. *J. Am. Chem. Soc.* **1997**, *119*, 7350.

(107) Rayner, D. M.; Ishikawa, Y.; Brown, C. E.; Hackett, P. A. *J. Chem. Phys.* **1991**, *94*, 5471.